Genesis of Active Phase and Support Effect in Ultradispersed Mo Sulfide Catalysts

D. Ryaboshapka, T. Len, P. Bargiela, M. Aouine, C. Geantet, V. Briois, L. Piccolo, P. Afanasiev

Genesis of active phase and support effect in ultradispersed Mo sulfide catalysts.

Daria Ryaboshapka[1*], Thomas Len[1], Pascal Bargiela[1], Mimoun Aouine[1], Christophe Geantet[1], Valerie Briois[2], Laurent Piccolo[1], Pavel Afanasiev[1]*

[1]Univ Lyon, Univ. Claude Bernard Lyon 1, CNRS, UMR5256, IRCELYON, F-69626, Villeurbanne, France

[2]SOLEIL synchrotron, UR1-CNRS, L'Orme des Merisiers, BP48, 91192 Gif-sur-Yvette, France

Keywords: Ultradispersed metals; *operando* XAS; molybdenum sulfide; support effect;

Abstract

Molybdenum sulfide –based catalysts are widely used for hydrotreating, hydrogen evolution and many other reactions. Recently, we demonstrated that not only the edges of MoS_2 slabs, but few-atom ultradispersed MoS_x clusters possess high intrinsic activity. However, the structure and the genesis of such ultradispersed species remain unknown. Herein we present a comparative study of MoS_x catalysts ultradispersed on different supports (carbons, SiO_2, Al_2O_3, TiO_2). Evolution of the Mo species during sulfidation and HDS reaction was studied by means of operando Quick-X-ray absorption spectroscopy (QXAS) at the Mo K edge, assisted by chemometric analysis (MCR-ALS). Significant differences of the structure of Mo species and their temperature evolution as a function of support were observed. The sulfidation pathway involves formation of oxysulfide and sulfur-rich MoS_3-like intermediates, which are further transformed into the final MoS_x clusters. As compared with MoS_2 nanoslabs, the coordination numbers of Mo in the ultradispersed clusters are decreased and the interatomic Mo-S and Mo-Mo distances are shortened. Other characterizations, in particular STEM-ADF, confirm that few-atom clusters and single-atom (SA) species are predominant in all the catalysts. The materials show high activity per Mo atom in hydrodesulfurization (HDS) of thiophene, varying in step with the MoS_x dispersion as determined from XAS, in the sequence: Mo/carbons > Mo/TiO_2 > $Mo/Al_2O_3 \approx Mo/SiO_2$.

1. Introduction

Lamellar molybdenum sulfide MoS_2 is a well-known catalyst for hydrodesulfurization (HDS) reaction, used to remove sulfur from petroleum fractions.[1] For a long time it was considered that only the edge sites of hexagonal and triangular MoS_2 slabs are catalytically active.[2,3] Theoretical models predict the specific activity to depend on the amounts of exposed crystallographically distinct M- and S- edges.[4,5] Recent studies describe tuning the slabs shape, aiming at the control of M to S edge ratios.[6] However, some experimental results require to go

beyond the conventional 2D slabs model. Thus in the studies of model unsupported MoS_2 and supported MoS_2/Al_2O_3 catalysts,[7,8] the specific HDS activity did not evolve in step with the amount of exposed edges as estimated from TEM. Moreover, as the STEM-HAADF technique became widely used for studies of supported sulfides, the features smaller than 1 nm or even single atoms were systematically observed alongside the MoS_2 slabs.[9, 10, 11] These subnanometric or single atomic features persisted even after the thiophene HDS test at 350 °C.[10] However, the catalytic activity of such species was never accessed. Recently, combining a high –surface activated carbon support, low Mo loading and a simple adsorption preparation technique, we prepared MoS_x/C catalysts that contained no TEM-detectable slabs, but mostly SAs and subnanometric clusters.[12] These catalysts demonstrated high specific HDS activity and high degree of promotion with cobalt. However, the structure of ultradispersed MoS_x species in the conditions of HDS reaction remained unclear, because merely *ex-situ* XAS measurements were carried out in our previous work.[12]

The support effect in the conventional sulfide HDS catalysts has been widely studied for a long time.[13,14,15,16] The nature of the support strongly influences the MoS_2 slabs size, stacking, orientation as well as the coordination of Mo atoms.[17,18,19,20] Several (not mutually excluding) models of the support effect were proposed, focusing on different properties, such as the support acidity,[21,22] its impact on the MoS_2 slabs dispersion via interactions in the oxidic form,[23] its impact on the reducibility of slabs edges,[24] different properties of exposed crystallographic facets of support particles,[25] or the electronic effects.[26,27] In all these models nanoparticulate monolayer or stacked MoS_2 particles were considered, in which only a minority of Mo atoms is potentially involved in the interaction with a support. To observe the support effect by physical techniques, the greater possible part of the active phase (MoS_2) should interact with the support, i.e. the greater is the dispersion of the active phase, the higher should be the observed effect. Therefore in the ultradispersed MoS_x catalysts, a strong influence of support on the properties of the supported sulfide species could be expected.

Since the active species of sulfide catalysts are air-sensitive, in-situ and operando techniques are the most appropriate to characterize them. X-ray absorption spectroscopy (XAS), due to its element-specificity and relatively high penetration of hard X-rays through the catalyst, is one of the most valuable techniques to study sulfide catalysts upon activation and under working conditions.[28] Dynamic conditions of temperature and gas atmosphere during sulfidation and reaction cause chemical transformations, from the oxide precursor to the final sulfide active phase, stable under reaction conditions. In earlier works, in-situ XAS was applied to study genesis of active phase in the unpromoted and Co-promoted Mo-based hydrotreating catalyst.[29,30] Recently,

due to the use of time-resolved quick XAS (QXAS) and chemometry techniques of data analysis (MCR ALS) unraveling between the intermediate species during the catalyst activation become possible.[31,32] While XAS operando was widely applied to follow the genesis of conventional alumina supported (Co)Mo catalysts, it was never used to systematically study the support effect, neither to characterize the ultradispersed sulfide species.

The present study is focused on the properties of ultradispersed Mo sulfide species formed during the sulfidation and HDS reaction on several widely studied supports, including carbons, SiO_2, Al_2O_3 and TiO_2. To obtain insights into the nature of the Mo species evolution, we applied *operando* quick X-ray absorption spectroscopy (QXAS) technique in combination with chemometric data treatment approach.

2. Experimental

2.1. Preparation of the catalysts

All reactants and solvents were high-purity-grade products purchased from Sigma Aldrich. Four supports were used: Activated Charcoal Norit (AC), graphene flakes (Sigma Aldrich), TiO_2 (PC500 anatase, Evonik) and γ-Al_2O_3 (Prolabo). The silica-incorporated Mo-KIT-6 sample was homemade (vide infra). Different preparation techniques and different Mo precursors were applied to prepare the catalysts, in order to ensure the highest possible dispersion of Mo oxide species. We supposed that if the initial Mo oxide species are ultradispersed, it would maximize the Mo species dispersion during the following sulfidation. On the other hand if nanoparticles of Mo oxide phase were formed in the initial state, then further sulfidation would probably lead to poorly dispersed sulfide phase. For this reason, conventional impregnation was not applied for carbons and silica that contain low amounts of surface functional groups and tend to stabilize poorly dispersed supported oxide species. To avoid agglomeration, the supports with specific surface areas were applied and the loading of Mo precursor was relatively low, corresponding to the calculated value of 1 wt% Mo (see Table S5 for the chemical analysis results).

Mo/AC and *Mo/graphene* samples were prepared *via* equilibrium adsorption route applied in our previous work.[12] A weighted amount (27.0 mg) of $(NH_4)_2MoS_4$ was dissolved in methanol and added dropwise to a suspension of 1g carbon in 100 mL of methanol, under continuous stirring. After 4 h of stirring red color of thiomolybdate solution disappeared and adsorption was considered complete. The samples were then filtered and dried under Ar flow at room temperature. Note that even if a thiosalt was used as precursor, this preparation leads to ultradispersed supported oxide species.[12]

Mo/TiO_2 and *Mo/Al_2O_3* were prepared via conventional impregnation techniques that already afforded ultradispersed oxidic Mo species in our previous works (but for higher Mo

loadings).[33] A calculated amount (18.3 mg) of $(NH_4)_6Mo_7O_{24}.4H_2O$ (AHM) was dissolved in a volume of distilled water equal to the pore volume of the support. Then, the solution was added dropwise to 1 g of the support powder and mixed vigorously for several minutes. The solids were dried in oven for 3 h at 110 °C. Reference MoS_2/Al_2O_3 with 10 wt% Mo loading was synthesized by impregnation with AHM with addition of citric acid according our previous work.[34] It is further designated as $10Mo/Al_2O_3$. 10 wt% Mo references on other supports were prepared using impregnation with AHM followed by drying, as for Mo/Al_2O_3.

Mo-KIT-6 (Mo –incorporated mesoporous silica) was prepared according to the literature procedure,[35] where predominance of di- and monomolybdate species was evidenced. In brief, 19 g of 2 M HCl was mixed with 2 g Pluronic P-123 (Mw 5800) and stirred until the P123 full dissolution. Then 33.8 mg of AHM in 50 g deionized water was added to the template solution. After stirring for 2 h, 2.5 g *n*-butanol was added and kept stirring for 1 h more. Finally, 6.4 g TEOS was added dropwise. After stirring for 24 h, the solution was transferred to a Teflon-lined autoclave and treated for 24 h at 100 °C. After filtration, drying at 100 °C for 6 h and calcination in air at 550 °C for 6 h, the Mo–KIT-6 solid was obtained.

Before HDS reaction the samples were sulfided in a Pyrex reactor under 15%vol. H_2S/H_2 gas mixture flow (0.6 $L.h^{-1}$ H_2S, 3 $L.h^{-1}$ H_2) at 350 °C for 1 h and heating rate 5 $°C.min^{-1}$. When sulfidation was finished, the H_2S flow was turned off and the samples were cooled to room temperature in a 1.8 $L.h^{-1}$ flow of H_2. Afterwards the samples were handled and stored under argon.

The designation of the samples is as follows: (i) – stands for the initial (oxide) sample; (s) – sulfided, sample after sulfidation; (h) – sample taken after HDS reaction, e.g.: Mo/Al_2O_3-i, Mo/Al_2O_3-s, Mo/Al_2O_3-h.

2.2. Thiophene HDS test

A weighted amount of a freshly sulfided sample was placed in a flow fixed-bed Pyrex microreactor. A 3 $L.h^{-1}$ H_2 flow passed through a saturator containing liquid thiophene at 0 °C. The reaction was performed at atmospheric pressure at three different temperatures: 320, 330, 340 °C. Steady-state conversions were estimated after at least 16 hours on-stream. The reaction products were analyzed by gas chromatography on an Agilent 7820A device equipped with a flame ionization detector. The HDS rates per unit of catalyst mass were estimated according to the equation (1),

$$r = -(\frac{F_{thio}}{m}) \times \mathrm{Ln}(1 - X)\,, \qquad (1)$$

where r is the specific HDS rate, F_{thio} is thiophene molar flow ($mol.s^{-1}$), m is mass of the catalyst (g) and X is thiophene conversion.

Specific activity values per Mo atom were calculated using equation (2):

$$Specific\ activity = \frac{r \times N_A}{N}, \quad (2)$$

Where r is specific HDS rate per mass unit (mol.g^{-1}s^{-1}), N_A is Avogadro number and N is number of Mo atoms per gram of the catalyst.

2.3. Characterizations

Mo content in the samples was determined by inductively coupled plasma-optical emission spectroscopy (ICP-OES, Activa instrument from Horiba Jobin Yvon). The carbon supported samples were dissolved in H_2SO_4 and HNO_3 mixture and heated to 300 °C, while for the samples on the oxidic supports the H_2SO_4 - HNO_3 -HF mixture was used. Phase composition was studied by powder X-ray diffraction (XRD) on a Bruker D8 Advance A25 diffractometer with CuKα emission. The crystalline phases were identified by comparison with the JCPDS standards. Specific surface area and porosity were studied by means of N_2 adsorption-desorption at -196 °C on a Micrometrics ASAP 2010 device and calculated using BET and BJH equations. Prior to measurements the samples were degassed at 350°C for 2 h. Transmission electron microscopy (TEM) was carried out on a JEOL 2010 FEG instrument at an accelerating voltage of 200 kV. STEM-ADF images were obtained on a FEI Titan G2 aberration-corrected environmental TEM device operating at 300 kV. Prior to characterization, the catalysts were crushed in agate mortar with addition of a small amount of ethanol, then the obtained suspension was ultrasonicated for several minutes. Then, a droplet of suspension was placed on a holey carbon–covered copper grid and dried. The images obtained by TEM and STEM were analyzed with the Digital Micrograph Gatan program package. Raman spectra were obtained on a LabRam HR spectrometer (Horiba-Jobin Yvon). The samples were put in a homemade sample holder under Ar atmosphere, to protect them from oxidation. Prior to measurements the spectrometer was calibrated using silicon reference. Ar laser with λ = 532 nm was applied as excitation source. The spectra were accumulated during different periods of time, from 10 to 1800 s. UV-visible Diffuse Reflectance UV-visible diffuse reflectance spectroscopy (UV-vis DRS) was performed on Perkin Elmer Lambda 45 UV/VIS Spectrometer. 20 mg of each sample was mixed in an agate mortar with 1 g of $BaSO_4$ and placed into a UV-vis cell. The spectra were recorded in the reflectance mode in the wavelength range from 1000 to 200 nm. The measured reflectance (R) was transformed to Kubelka-Munk function via the equation (3):

$$F(R) = \frac{(1-R)^2}{2R} \quad (3)$$

Where R is reflectance.

X-band (9.5 GHz) EPR spectra were recorded at 77 K on a Bruker ESP 300E spectrometer using a standard rectangular (TE102) EPR cavity (Bruker ER4102ST). Microwave power of 1.6 mW and modulation amplitude of 1 G were used. Visualization of the structures initial Mo species and of their transformation during sulfidation was performed using the Avogadro software (ver. 1.2.0.). The geometry of the species was approximately optimized with Molecular Mechanics feature (for presentation purposes only).

X-ray photoelectron spectroscopy (XPS) measurements were performed on a Kratos Axis Ultra DLD spectrometer the monochromatic Al Kα radiation (1486.6 eV) was used as X-ray source, operating at 180 W, 15 kV, 12 mA. Before the measurement, the powders of sulfided samples were placed on a conductive carbon tape under Ar atmosphere. The survey spectra were registered in the interval 1200 – 0 eV with a pass energy 160 eV. High-resolution spectra at a pass pass energy of 40 eV, were obtained for O 1s, Mo 3d +S 2s, C 1s and S 2p regions (the spectra Ti 2p for Mo/TiO_2, Al 2s for Mo/Al_2O_3 and Si 2s for Mo-KIT-6 were also acquired). The treatment of the XPS spectra was performed with CasaXPS software. For spectra alignment, C 1s photoemission peak of adventitious carbon (sp^2 carbon) located at 284.8 eV was used.

2.4. Operando QXAS study

The coordination environment of Mo was studied by means of X-ray absorption spectroscopy (XAS) in the transmission mode at the SOLEIL synchrotron facility, ROCK (Rocking Optics for Chemical Kinetics) beamline.[36] A weighted amount of powder of an initial sample was placed into the cavity in the sample holder between two graphite layers. The sample holder was then inserted into the special cell for *operando* characterizations. More details on the sample holder and the cell might be found in Ref.[37] The spectra were recorded at Mo K edge using a Si(111) channel-cut monochromator aligned at 5.65° and oscillating at 2Hz frequency with an amplitude of ≈ 0.4°. Harmonics were rejected using Pd mirrors with a 2.8 mrad grazing incidence compared to the pink and monochromatic beams delivered by the toroidal collimating mirror and the channel-cut monochromator, respectively. A set of 3 ionization chambers filled with 50:50 $Ar:N_2$ mixture was used for measuring the sample transmission and the transmission of a Mo metallic foil used as internal absolute energy calibration.

The spectra were recorded during the samples treatment in the following sequence: (1) the initial sample was put under Ar flow; (2) H_2 and H_2S were introduced into system and the sulfidation/reduction was performed via heating up to 350 °C, heating rate 5 $°C.min^{-1}$; (3) the sample was maintained at 350 °C for 1 h; (4) H_2S flow was switched off and thiophene was introduced to perform HDS reaction for 4 h; (5) thiophene was switched off and the sample cooled

to room temperature in H_2 flow, rate 20 °C.min^{-1}; (6) H_2 flow was switched off and the system was purged with Ar.

Preliminary data treatment was performed using the ATHENA software.[38] Fitting of the EXAFS spectra was carried out with VIPER program both in k (BFT) and R spaces.[39] The R-space fitting was performed in the (Im+Module) mode. During the fitting procedure the values of R (distance), CN (coordination number), σ^2 (distance variance) and ΔE_0 (energy difference) were varied. The goodness of the fit was determined by the value of R-factor.

To analyze the intermediate species appearing during the sulfidation we applied a set of chemometric data analysis tools.[40] All procedures were performed with Matlab R2021a software. First, we constructed a matrix of normalized XAS spectra recorded during a specific process (sulfidation, reaction…) with a merge over 15 s of the data recorded successively during the heating ramp and over 300 s for the data recorded during isothermal treatment. The normalization of the raw data was performed using the homemade Normal GUI interface available at the beamline.[41] The normalized data were assembled as a matrix using a homemade XAS-SVD Matlab GUI toolbox which allows for a preliminary PCA (Principal Component Analysis) estimation of the number of components from the scree plot of eigenvalues. Afterwards, MCR-ALS (Multivariate Curve Resolution – Alternating Least Square) was applied on the matrix obtained in XAS-SVD, to extract pure components and their concentrations.[42] Evolving Factor Analysis (EFA) allowed the initial estimation of concentration profiles.[43] After the initial estimation certain constrains were applied in the ALS algorithm, including unimodality, non-negativity and evolution interval from 0 to 100% for concentration profiles and non-negativity for the spectra. Then MCR-ALS performed reconstruction of the initial data matrix using the obtained pure components.

3. Results and Discussion

3.1. Properties of the sulfide catalysts accessed by physical techniques.

Most characterizations were performed on the freshly sulfided samples, unless otherwise stated. Textural characterizations for bare supports and chemical analysis results for sulfided solids are provided in Fig S1 and Table S1 respectively. The XRD patterns of sulfided samples (not shown) contain only the reflections of bare supports. Raman, EPR and XPS spectroscopies were applied on the samples sulfided ex-situ without air admission. Other ex-situ methods (UV-vis DRS, XRD, conventional TEM and STEM-HAADF), that could be implemented only after a short air exposure, are useful to access dispersion of Mo species, but partial oxidation is possible.

Raman spectroscopy

Raman spectra were recorded in an *in-situ* reactor, under static Ar. The spectra of bulk or nanoscopic MoS_2 usually show two intense peaks at 383 cm^{-1} and 408 cm^{-1}, corresponding to the E_{2g} and A_{1g} modes.[44, 45] For Mo/AC-s and Mo/graphene-s, no signal could be detected between 300 and 500 cm^{-1} even for long acquisition times, but only two intense peaks were spotted at 1321 and 1598 cm^{-1}, characteristic of defective carbon (Fig. S2a). For Mo/TiO_2-s, the region of interest contains intense lines of TiO_2 anatase at 396, 516 and 635 cm^{-1} (Fig. S2b). Poorly resolved broad lines around 354 cm^{-1} and 409 cm^{-1} were observed for Mo/Al_2O_3-s and around 361 cm^{-1} and 412 cm^{-1} for Mo-KIT-6-s (Fig. S2c). These features resemble MoS_2, but are shifted and strongly broadened, suggesting that Mo species are highly disordered MoS_2 clusters. The peaks located around 215 cm^{-1} for Mo/Al_2O_3-s and 210 cm^{-1} for Mo-KIT-6-s are close to the line at 227 cm^{-1}, attributed to disorder in the MoS_2 nanoslabs.[46] Weak signals at 970 cm^{-1} and 840 cm^{-1} Mo-KIT-6-s suggest partial oxidation of Mo sulfidic species.[47] A weak line at 970 cm^{-1} observed for pure KIT-6 corresponds to a Si-OH vibration.[35] For Mo/Al_2O_3-s a small peak at 920 cm^{-1} might be ascribed to Mo=O stretching in the supported molybdate.[48,49] Overall, Raman spectra suggest the presence of highly disordered MoS_2-like clusters in Mo-KIT-6-s and Mo/Al_2O_3-s, whereas for Mo/AC-s, and Mo/graphene-s no signals of Mo sulfide species could be spotted. For Mo/TiO_2-s, a strong signal from the support would anyways hide the peaks of the sulfide species**.**

UV-vis DRS

UV-vis DRS spectra were recorded only for the oxides - supported samples, because carbon-supported samples are black. In bulk MoS_2, direct electronic transitions between conduction band and valence band result in two absorption peaks around 610 and 670 nm.[50, 51] For the MoS_2 catalysts supported on alumina, silica and titania, the UV -vis peaks of MoS_2 were observed and easily distinguished from those of the corresponding supports even in air.[52, 53, 54,55] In our spectra, beside the absorption bands of supports, several broad peaks centered around 420, 470 and 570 nm were observed, but no bands were present above 600 nm (Fig. S3). This difference might be explained by ultradispersion of MoS_x species, leading to modification of their electronic properties, or due to partial oxidation of MoS_2 nanoclusters in air.[56] Therefore our UV-vis DRS results corroborate the absence of MoS_2 slabs.

X-ray photoelectron spectroscopy (XPS)

The XPS spectra were obtained for the sulfided samples without air exposure. For all samples single Mo species were detected, with the binding energy (BE) $3d_{5/2}$ varying in the interval 228.0 – 229.3 eV (228.8 eV for Mo-KIT-6-s, 228.6 eV for Mo/Al_2O_3-s, 229.3 eV for Mo/graphene-s, 229.2 for Mo/AC-s,[12] and 228.6 eV for Mo/TiO_2-s). A variance in BE exists as a function of

support (up to 0.6 eV). Typical BE $3d_{5/2}$ for Mo(IV) in MoS_2 is around 229 – 229.2 eV[57, 58] and here we observe the same energies for Mo/AC-s and Mo/graphene-s. The BE was slightly decreased for Mo/Al_2O_3-s, Mo-KIT-6-s and Mo/TiO_2-s. The lower binding energy values correspond to the MoS_{2-x} sulfur-deficient species.[59]

The S 2p spectra are different depending on the nature of the support. For Mo-KIT-6-s, due to low Mo loading, a strong Si 2s signal and the corresponding plasmon hide the S 2p line. On graphene and AC, S^{2-} and S_2^{2-} species were identified with BE $2p_{3/2}$ around 162.3 and 164.1 eV respectively.[60] On the surface of Al_2O_3 and TiO_2 oxides, along with S^{2-} and S_2^{2-}, oxidized sulfur species with BE $2p_{3/2}$ at 168.1 and 166.7 eV were also present (SO_4^{2-}, SO_3^{2-}), despite the fact that all samples were prepared for XPS under Ar. A contribution of SO_x species on the oxidic supports might be related to sulfur species on the supports surface. As the Mo loading is low, the S signal coming from the sulfur species adsorbed on the supports becomes non-negligible. The XPS Mo/S atomic ratio in the oxide-supported samples is greater than two (Table S2) and therefore a major part of S species is not associated with molybdenum, but bonded with the oxygenated supports moieties, prone to form oxygenated sulfur species.

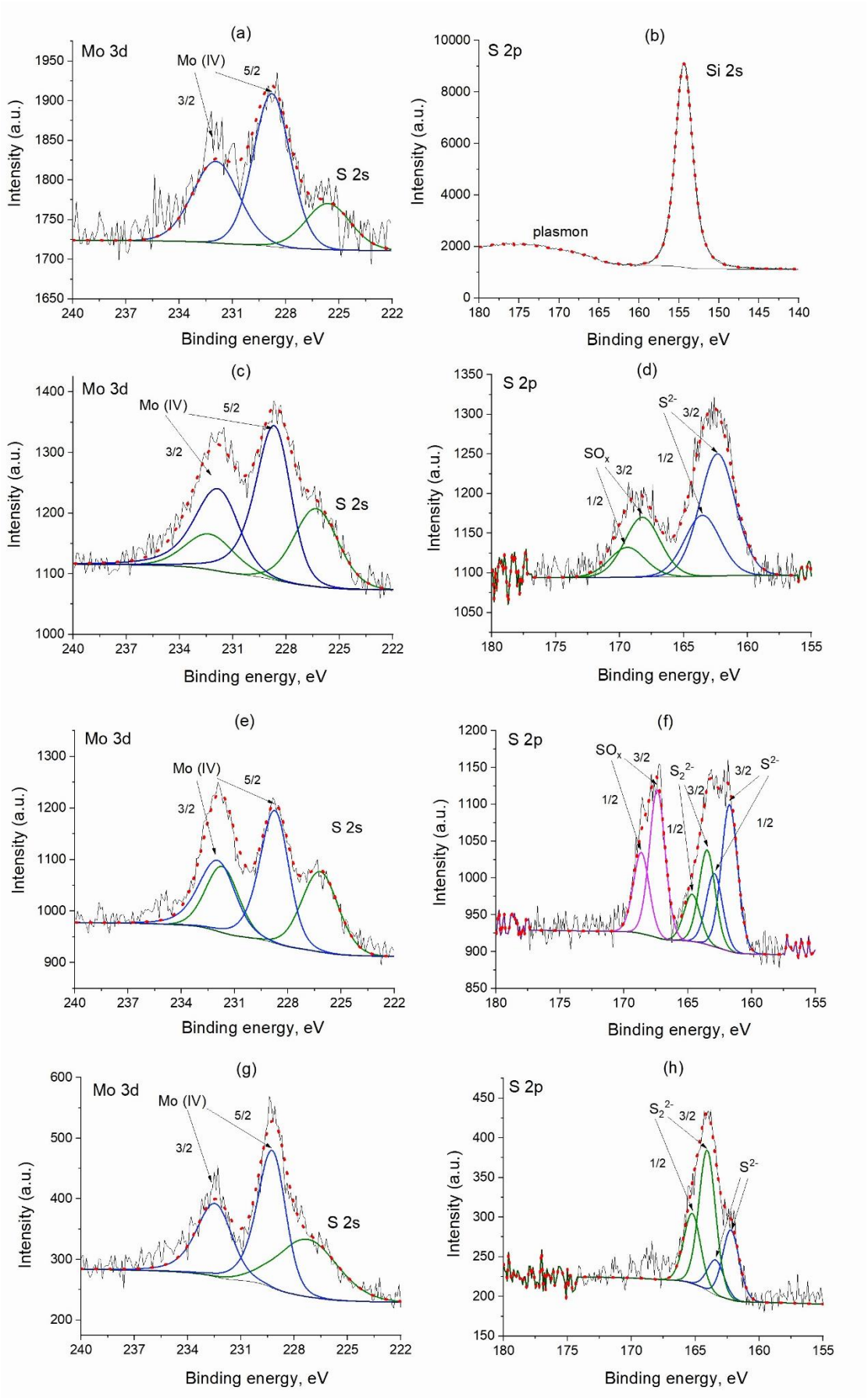

Figure 1. XPS spectra for Mo-KIT-6-s (a-b), Mo/Al_2O_3-s(c-d), Mo/TiO_2–s (e-f), Mo/graphene-s (g-h).

Transmission electron microscopy (TEM) and scanning transmission electron microscopy (STEM-ADF).

TEM and STEM-ADF were carried out *ex situ* for the sulfided samples. For the Mo-KIT-6-s, mesoporous ordered structure of the support was revealed at medium magnifications by TEM and STEM (Fig. S4), but at high magnifications the TEM images were featureless (Fig. S4a, b). For the Mo/Al_2O_3-s, only acicular γ-Al_2O_3 particles were spotted with interplanar distances 0.26 nm, corresponding to the (2 2 0) planes (Fig. S5c, d). Small (5-10 nm) oxide nanoparticles were observed for Mo/TiO_2-s, showing the (1 0 1) planes of anatase at 0.35 nm spacing (Fig. S5e, f). Only graphite (002) planes with 0.338 nm spacing were visible on the Mo/AC-s and Mo/graphene-s (Fig. S5g, h; Ref. 12). Meanwhile, EDS analysis confirms that Mo is present in all these samples, uniformly spread over the analysis zones (Fig. S6). Therefore, the Mo species are smaller than the size detectable by conventional TEM. Notably, detection of 1-2 nm length MoS_2 slabs in the conventional supported catalysts is a routine task, while using the same microscope and the same observation conditions.[35] In the TEM and STEM images of 10 wt% Mo references, abundant MoS_2 slabs were easily detected (Fig. S7).

The STEM-ADF technique allows distinguishing small Mo-containing species from lighter atoms of supports (C, O, Al, Si, Ti), due to a strong Z-contrast. Mostly single atomic species and agglomerates of several atoms were observed in our samples (Fig. 2 and Fig. S8). The dispersion of Mo species seems to be different as a function of support. Thus, for Mo supported on both carbons and TiO_2 only small subnanometer clusters were observed (Fig. 2g, h, c, d, Fig. S9, Ref. [12]), whereas for Mo/Al_2O_3-s and Mo-KIT-6-s nanometer-sized Mo clusters were encountered (Fig. 2a, b, e, f). Statistical treatment of images suggests that the Mo species on carbons and TiO_2 are more dispersed than on alumina and silica (Fig. S9, S10).

In summary, we evidenced that ultradispersed MoS_x species are present in the samples under study. However, only *operando* characterization allows obtaining reliable structural information under controlled conditions. Therefore, we proceeded with *operando* QXAS study of our systems, as follows.

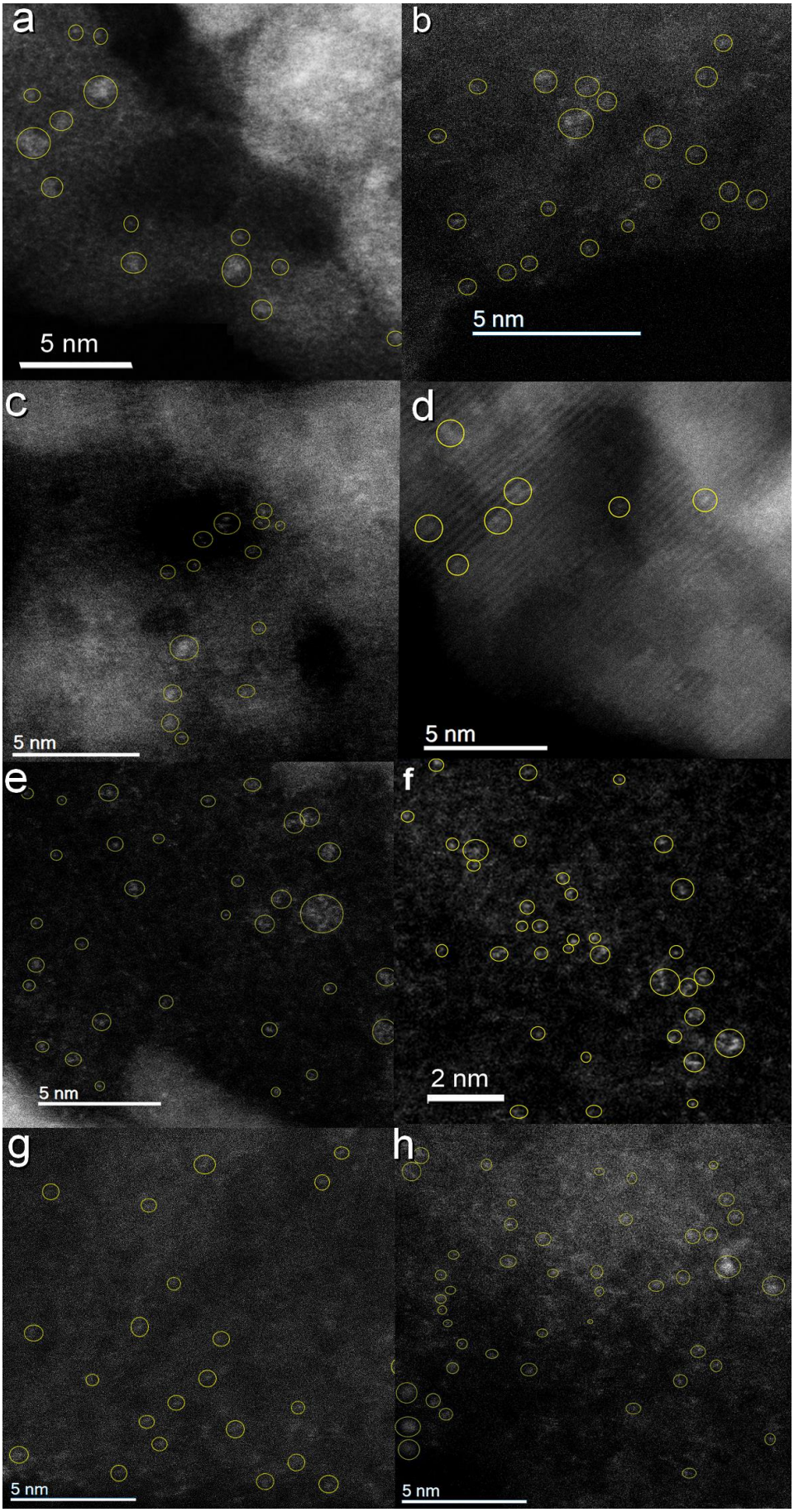

Figure 2 STEM-ADF images of Mo-KIT-6-s (a,b), Mo/TiO_2-s (c,d), Mo/Al_2O_3-s (e,f), Mo/graphene-s (g,h). Selected Mo clusters and SA are marked with circles.

3.2. Operando QXAS investigation

Operando QXAS study aimed to clarify the structure of the ultradispersed species, their genesis during the sulfidation step and their evolution during the HDS reaction. We inquired whether the obtained sulfide species are similar to the conventional sulfide structures or not, and how the nature of the support influences their genesis. Drastic changes of XAS spectra occurred during the sulfidation, but almost no evolution was observed during the following HDS reaction (Fig. S11, 12). Therefore, the discussion is focused mostly on the sulfidation step.

3.2.1. The initial and the final states

Fig. 3 and Table 1 summarize the results of XAS study for the initial samples. For all samples, the initial Mo species are monomers or few-atom oxidic clusters. However, the structure of Mo species varies considerably as a function of support. Monomeric molybdate is predominant on alumina, whereas polymolybdates (probably aluminium hexamolybdate) are present in the 10 wt% Mo/Al_2O_3-i reference, in agreement with the literature.[61] On both carbon supports dimeric "Mo blue" species were formed as described in our previous work.[12] On the oxide supports, different species are formed despite the same precursor (AHM) and the same Mo loading, in agreement with earlier studies on the support effect.[13,14,15] Alongside monomers, some silicomolybdic (Keggin) anions are probably present in the Mo-KIT-6-i sample, easily formed by the reaction between the dissolved $Mo_7O_{24}^{6-}$ and silica surface, so expected to be produced in the conditions applied for the preparation.[62,63] In the Mo/TiO_2-i, polymeric species coexist with monomers, despite low Mo loading and high specific surface area of the TiO_2 support. A pre-edge is present in the XANES of all initial samples, attesting a non-centrosymmetric coordination environment (Fig. S13). Detailed characterization and discussion of the oxidic Mo species on different supports is beyond the scope of this study. In general, the state of the initial Mo oxidic species is defined by such properties of the support as the value of isoelectric point (IEP), the nature and abundance of surface functional groups and the specific surface area, as demonstrated in many earlier works using vibrational spectroscopies and XAS.[64, 65, 66, 67]

The final sulfided state was attained in all samples during the temperature increase step and showed no further evolution during the subsequent temperature plateau (1 h at 350 °C in H_2S/H_2 flow). The spectra acquired in H_2S/H_2 at 350 °C and the results of fitting are shown in Fig. 4 and Table 2. The coordination number (CN) values in Table 2 attest that in none of the samples Mo atom had a complete MoS_2-like shell of six S atoms. Moreover, the spectra of all low–loaded samples demonstrate drastic differences as compared with the 10 wt% Mo/Al_2O_3-s reference: the Mo-S and Mo-Mo coordination numbers are considerably lesser, whereas the Mo-S and Mo-Mo distances are slightly shortened vs. the reference, which contains highly dispersed, but TEM-

observable MoS_2 slabs.[34] This agrees with formation of ultradispersed species: upon an increase of dispersion the coordination numbers should decrease, whereas contraction of chemical bonds in the small clusters is generally expected vs. the corresponding bulk materials.[68]

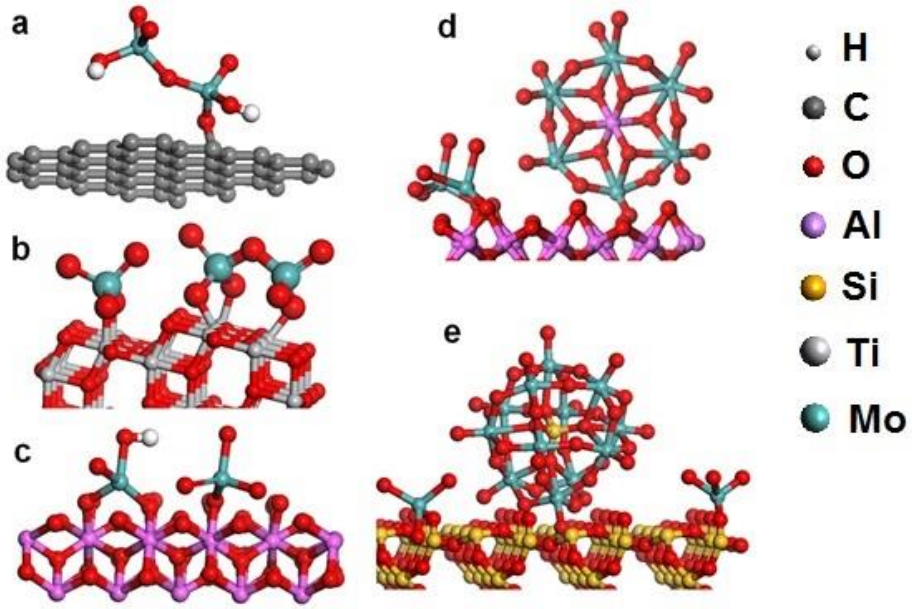

Figure 3 Illustration of the possible structures for the initial Mo oxide species on (a) carbon; (b) TiO_2; (c) Al_2O_3; (d) 10% Mo/Al_2O_3-i reference; (e) KIT-6.

Table 1 EXAFS fitting results for the initial oxide samples

Scatterer atom	*CN*[a]	*R(Å)*[b]	σ^2 (Å^{2bc}	ΔE_0 (eV)[d]
Mo/graphene-i R= 0.09				
O	2.1(2)	1.70(3)	0.004(1)	1(2)
O	1.6(5)	1.93(2)	0.004(1)	1(2)
Mo	1.7(2)	3.26(2)	0.006(1)	0(2)
Mo/AC-i R=0.17				
O	2.2(3)	1.71(2)	0.004(1)	-1(2)
O	1.5(3)	1.92(2)	0.005(1)	0(3)
Mo	1.8(2)	3.29(3)	0.005(1)	-1(2)
Mo/TiO_2-i R=0.19				
O	1.7(3)	1.72(3)	0.004(1)	5(3)
O	1.6(3)	1.95(2)	0.005(1)	1(2)
Mo	1.0(2)	2.91(2)	0.006(1)	1(2)
Mo	0.7(2)	3.34(2)	0.007(1)	-1(2)
Mo/Al_2O_3-i R= 0.07				
O	3.7(4)	1.75(2)	0.004(1)	0(1)
Mo-KIT-6-i R= 0.18				
O	1.4(2)	1.69(2)	0.004(1)	0(2)

O	1.5(2)	1.93(2)	0.004(1)	-1(2)
O	1.9(3)	2.37(3)	0.006(1)	-3(2)
Mo	2.2(2)	3.43(2)	0.007(1)	0(2)
10Mo/Al_2O_3-i reference R=0.12				
O	2.3(3)	1.71(3)	0.004(1)	1(2)
O	1.0(2)	1.94(1)	0.004(1)	0(1)
O	1.2(2)	2.36(2)	0.005(1)	0(2)
Mo	1.0(2)	3.40(2)	0.006(1)	1(1)

[a] coordination number, using S_0^2 = 1.0; [b] radial distance; [c]distance variance (free variable between 0.003 and 0.010); [d] energy variance (free variable between -10 and 10 eV), R-factor – minimized function of the fitting parameters, characterizes the goodness of the fit.

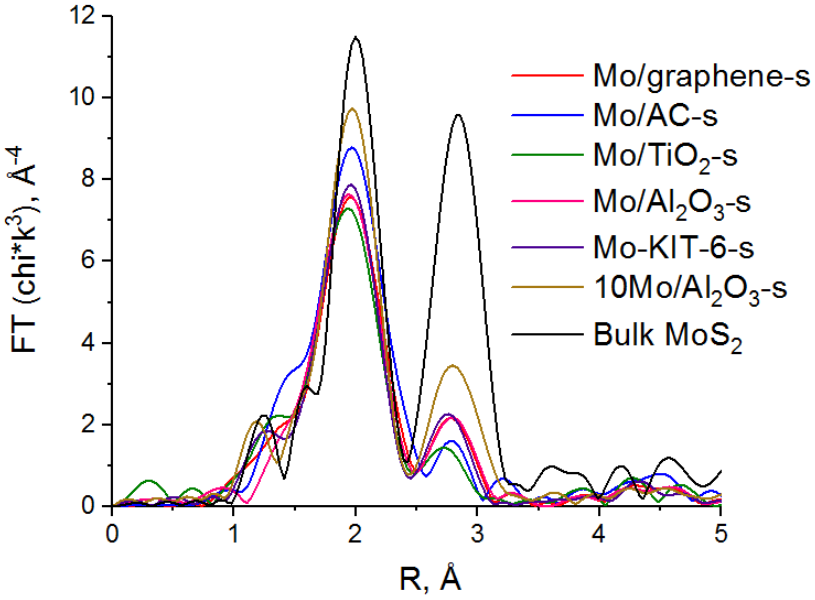

Figure 4 Experimental EXAFS spectra recorded in H_2S/H_2 at 350 °C, compared with 10Mo/Al_2O_3-s and bulk MoS_2 references.

The Mo/AC-s and Mo/TiO_2-s samples showed the strongest differences as compared with the 10Mo/Al_2O_3-s reference. In the Mo/AC-s sample, along with low Mo-S coordination number and negligible Mo-Mo one, some oxygen remained in the coordination sphere. In the Mo/TiO_2-s sample, the Mo-Mo distance of 2.78 Å corresponds rather to the short Mo-Mo bond observed in the amorphous MoS_x (x>3) than to MoS_2.[69] Three other samples (Mo/graphene-s, Mo-KIT-6-s and Mo/Al_2O_3-s) have similar EXAFS spectra with Mo-Mo CN ≤ 1 and Mo-S CN ≈ 4. The Mo-Mo distance though shortened (around 3.10 Å), is closer to that in the bulk MoS_2 (3.16 Å).

XANES spectra for sulfide samples are similar, as XANES of highly dispersed MoS_2 and amorphous MoS_x have similar shape and are relatively featureless (no pre-edge and no pronounced white line).[70] In summary, analysis of the EXAFS spectra after sulfidation suggests that dispersion of Mo species changes in the sequence: Mo/AC-s > Mo/TiO_2-s ≈ Mo/graphene-s > Mo/Al_2O_3-s ≈

Mo-KIT-6-s >> 10Mo/Al_2O_3-s. In the Mo/AC-s and Mo/TiO_2-s samples the Mo species significantly differ from the MoS_2 reference, whereas in Mo/graphene-s, Mo-KIT-6-s and Mo/Al_2O_3-s they might be considered as MoS_2-like few-atom clusters. Remarkably, there is no correlation between the XAS-derived dispersion of Mo species and physical properties of supports, reported as being important for the MoS_2 phase dispersion. Indeed, subdivision into "weakly" and "strongly" interacting ones cannot be a guideline. Thus, carbon, considered as a "weakly interacting" support[71] gives the most dispersed species, whereas "strongly interacting" titania and alumina give respectively the second highest and the least dispersed Mo sulfide species. On the other hand, our results are in a general agreement with the previous experimental works on conventional sulfide catalysts, where the same supports were compared. Thus, titania-supported MoS_2 was found to be better dispersed than alumina –supported one.[72] By the same token, carbon-supported MoS_2 was better dispersed and more active than silica- or alumina- supported one.[73]

Table 2 EXAFS fitting results for the sulfided samples (final state at 350 °C)

Scatterer atom	*CN*	*R (Å)*	*σ^2 (Å^2)*	*ΔE_0 (eV)*
Mo/graphene-s R= 0.09				
O	0.5(2)	1.94(3)	0.004(1)	3(2)
S	4.4(5)	2.39(2)	0.007(1)	3(2)
Mo	0.7(2)	3.09(2)	0.006(1)	-3(2)
Mo/AC-s R=0.09				
O	0.8(2)	2.00(4)	0.005(1)	-2(2)
S	3.1(3)	2.38(2)	0.009(1)	4(3)
Mo	0.2(2)	3.10(3)	0.005(2)	-3(3)
Mo/TiO_2-s R=0.11				
O	0.5(2)	1.94(3)	0.004(1)	-4(3)
S	4.1(4)	2.36(2)	0.007(1)	-3(2)
Mo	0.7(2)	2.78(2)	0.007(1)	-1(2)
Mo/Al_2O_3-s R= 0.10				
O	0.5(2)	1.95(3)	0.006(1)	-5(3)
S	4.4(5)	2.39(2)	0.007(1)	2(1)
Mo	1.0(2)	3.11(2)	0.006(1)	-4(3)
Mo-KIT-6-s R= 0.09				
O	0.1(2)	1.90(2)	0.004(1)	-2(2)
S	4.2(5)	2.39(2)	0.007(1)	0(2)
Mo	1.0(2)	3.11(2)	0.007(1)	2(2)
10Mo/Al_2O_3-s reference R=0.10				
O	-	-	-	-
S	5.2(3)	2.41(2)	0.006(1)	3(2)

Mo	2.3(3)	3.14(2)	0.006(1)	0(1)

The nuclearity of the initial oxide species was not correlated to that of the final sulfide ones: the most dispersed MoS_x was obtained from the dimers on AC and mixed monomers-oligomers on TiO_2, whereas the monomers prevailing in the initial Mo/Al_2O_3, were transformed to a lesser dispersed MoS_x. Therefore, during sulfidation, migration of Mo atoms and full reorganization their coordination sphere occur.

3.2.2. Sulfidation pathways

Many experimental and theoretical works on the genesis of MoS_2 from oxide precursors in the bulk and supported catalysts, converge on the conclusion that sulfidation is a multistep process involving intermediates. As suggested by Weber *et al.*, sulfidation of crystalline MoO_3 occurs via an oxysulfide low-temperature intermediate formed via exchange of terminal O^{2-} ligands of the oxide for S^{2-}. In the subsequent reactions, bridging S_2^{2-} ligands and Mo^{5+} centers are formed. Then, above 200°C, reduction with H_2 occurs, leading to oxygen elimination with formation of MoS_2.[74] For supported systems, formation of amorphous sulfur-rich MoS_3 -like intermediate was considered beside the oxysulfide one. Rochet et al studied sulfidation of alumina-supported molybdate by QXAS/MCR-ALS and concluded on the subsequent formation of two intermediates.[41] The first oxysulfide intermediate transforms into the MoS_3 – like second intermediate, that further decomposes to final MoS_2 phase.[75,76]

Recently, Raybaud and coll. studied the sulfo-reduction mechanisms of Mo oxide oligomers supported on γ-alumina by DFT and computed activation free energies of key chemical and diffusion steps. Interfacial O-atoms (Mo-O-Al) appeared as the most reluctant sites to be exchanged with S-atoms. S- and O-removal steps are kinetically too expensive on small-size Mo-oxysulfide oligomers. Formation of Mo trisulfide oligomers occurs prior to S-removal. An optimal path to MoS_2 via Mo trisulfide oligomers was proposed.[77]

The intermediates structure should obviously depend on the nature of the supported species and of the support, as well as on the sulfidation conditions. Low loading allows better revealing the support effect. Indeed, all the atomically dispersed Mo species in both the initial and the final states are involved in some interaction with the support.

Multivariate Curve Resolution with Alternating Least Squares (MCR-ALS) algorithm was used to separate large series of acquired spectra (usually 300-500 in our experiments) containing mixtures of initial/final products and reaction intermediates into their individual components and determine their concentrations during the sulfidation process. Assuming that the measured spectrum of the mixture can be represented as a linear combination of the spectra of pure

components scaled by their concentration, the algorithm iteratively alternates between the steps of pure spectra resolution and concentration estimation. At the end we treated the spectra of pure components in the same manner as experimental XAS and analyzed the concentrations profiles vs time or temperature, as follows.

Using the MCR-ALS procedure, four components accounting for the structural evolution of the catalysts under sulfidation conditions were identified, as presented in Fig. 5. Notably, this scheme does not require participation of hydrogen. Indeed, sulfidation with pure H_2S or H_2S/N_2 is known to provide supported MoS_2 catalysts with similar catalytic properties as sulfidation with H_2S/H_2.[35]

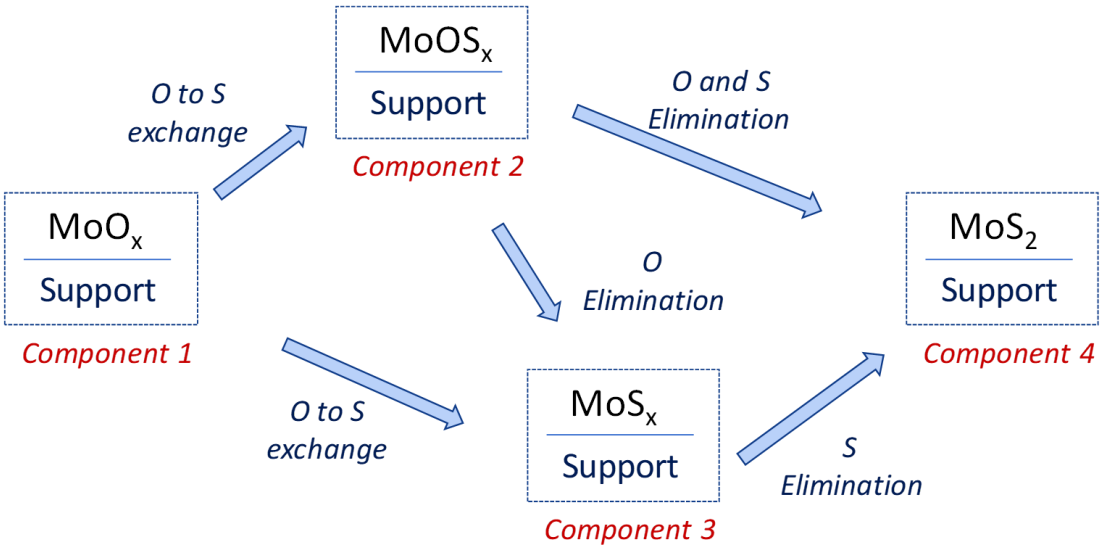

Figure 5 Scheme of sulfidation steps (as inspired by Ref. [79]) and the corresponding MCR-ALS components (see Fig. 7, 8).

In the following sections we describe the spectra of pure components as obtained by MCR-ALS on different supports and then compare their evolution.

1st components: The first component corresponds to the initial oxide species (Fig. 6a), already discussed above. It is worth mentioning difficult interpretation of the shell with the Mo-X distance above 2.3 Å, observed for 10%Mo/Al_2O_3-i and Mo-KIT-6-i (Table 1). Sometimes reported Mo-Al or Mo-Si intermetallic bonds[78] were ruled out, because they cannot be formed in the dried or air-calcined samples. The Mo-O-X (X= Ti, Al, Si) bonds in the heteropolymolybdates are much longer, in the range 3.2-3.5 Å (Fig. S14-16). Finally, we attributed this shell to the Mo-O bonds in polymolybdates, involving μ_3-oxygen. Such bonds with a length up to 2.3 – 2.4 Å exist in both AHM and $AlMo_6$ anions (Fig. S16).

2[d] components: The second component is an "oxysulfide" (Fig. 6b, Table S3). Its structure is strongly affected by the nature of the support (Fig. 7). For the "strongly interacting" Al_2O_3 and TiO_2, the Mo-O bonds are preserved in the Mo coordination shell, and fewer sulfur ligands are present, probably due to the persistent Mo-O-X species (X = Al, Ti). For the "weakly interacting" carbon supports, the degree of O to S exchange is higher. For Mo/AC, Mo/graphene and Mo-KIT-6, the second components are similar: Mo possesses four sulfur ligands, one residual oxygen and two types of Mo neighbors. One Mo – Mo distance at 3.38 Å is due to the remaining Mo – O – Mo moieties, while another one at 2.80 Å is typical for the Mo–Mo distances in sulfides, such as MoS_3.

Remarkably, for the Mo/Al_2O_3 sample the initial oxide species are monomers, but Mo-S-Mo bonds appear in the component 2. Therefore, the O to S exchange is accompanied by polymerization (Fig. 6a, b). The Mo=O to Mo-S exchange seems to be an easy process. In solutions, monomolybdate MoO_4^{2-} exchanges oxygen with sulfide ions at room temperature, forming oxothiomolybdates.[79] Apparently, at the surface of a catalyst, the Mo=S bonds, once formed, tend to oligomerize with reduction from Mo(VI) to Mo(V) and formation of S_2^{2-} species. Indeed, MoO_3/Al_2O_3 catalysts exposed to H_2S at room temperature become dark and show a strong Mo(V) signal in the EPR spectra (Fig. S17).

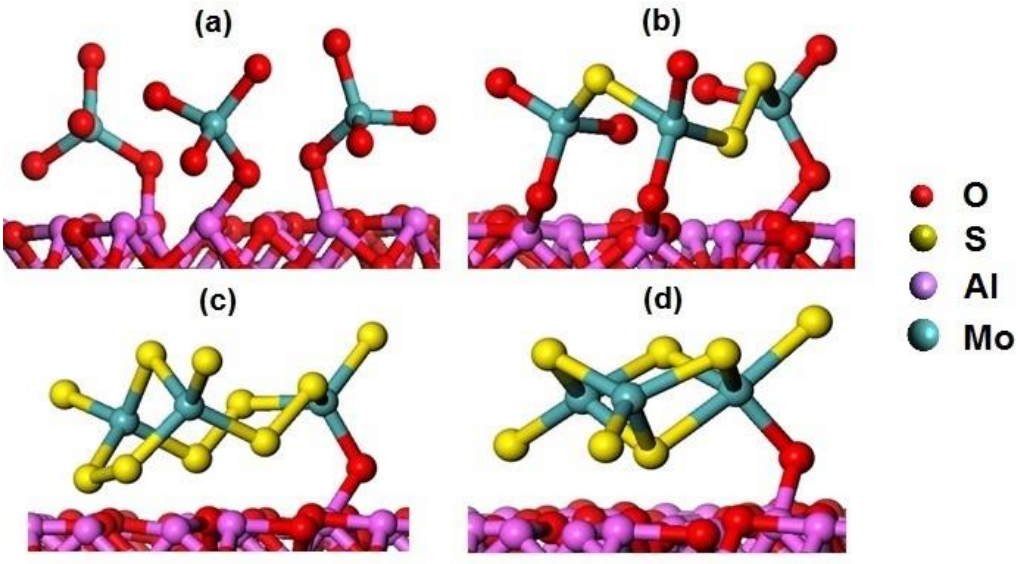

Figure 6. Illustration of the possible steps of sulfidation process as exemplified by Mo/Al_2O_3: (a) initial molybdate monomers (component 1); (b) oxysulfide species with (S_2^{2-}) bridges (component 2); (c) sulfur-rich MoS_3-like species (component 3); (d) MoS_2 – like structures (component 4). The structures are MM-optimized and given for visual presentation only.

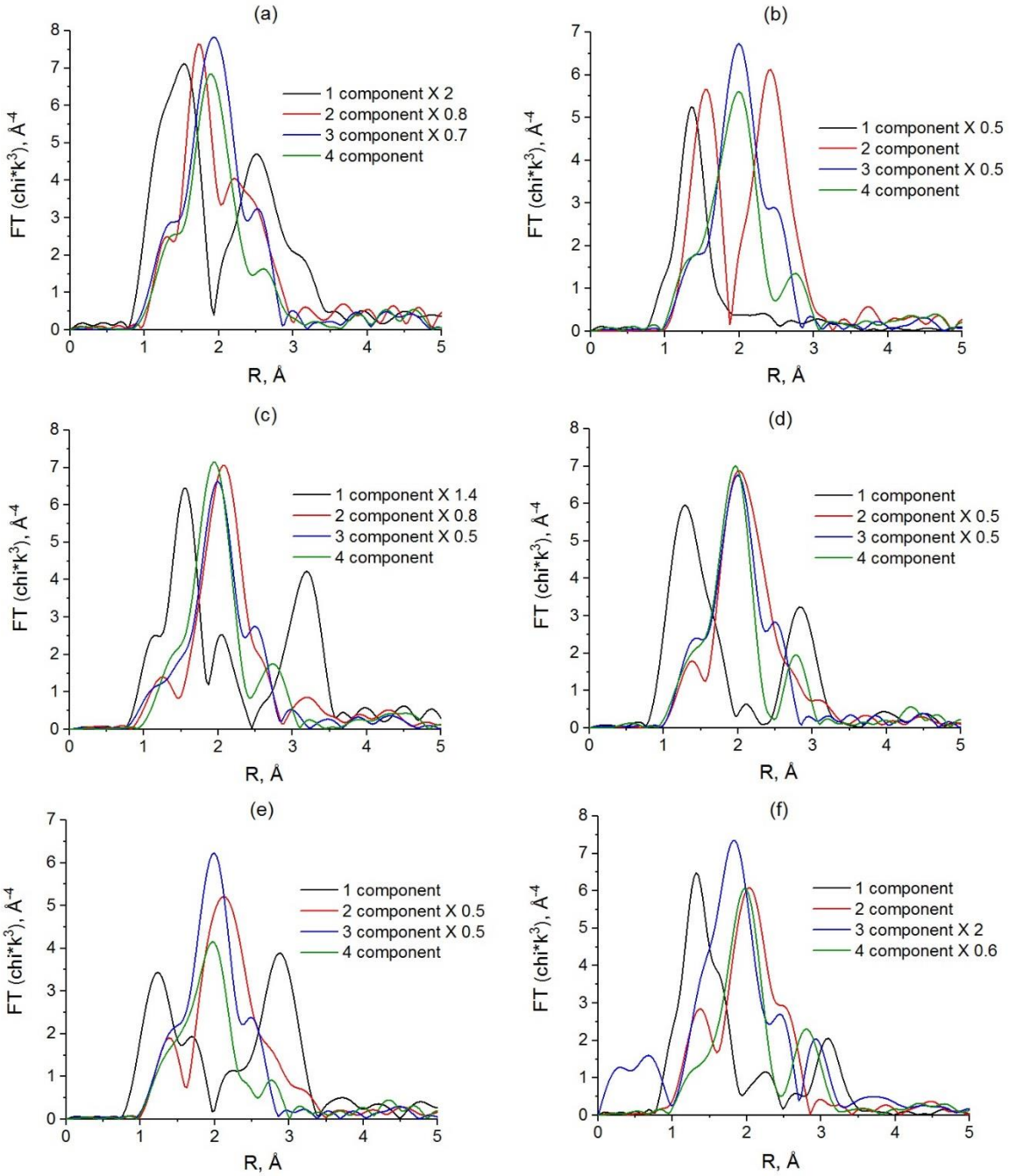

Figure 7. EXAFS spectra for all components for (a) Mo/TiO_2; (b) Mo/Al_2O_3; (c) Mo-KIT-6; (d) Mo/graphene; (e) Mo/AC; (f) reference 10Mo/Al_2O_3.

3^d components: The EXAFS spectra of the third components are similar for all samples. There is only a small contribution of oxygen (CN ≤ 0.6) at 1.65 – 1.71 Å due to the residual Mo-O bonds. The number of S ligands increases significantly (Table S3), whereas the Mo-O-Mo fragments disappear. The Mo-Mo distance is 2.76 Å, with CN ranging from 0.8 to 1.5. A sulfur-rich intermediate with MoS_3-like structure is therefore formed on different supports, in agreement with the previous studies.[40]

4^{th} components:

The fourth component is fully sulfided species, as discussed above. Note again a decreased Mo-S CN and shortened Mo-Mo and Mo-S distances for all ultradispersed catalysts as compared with the $10Mo/Al_2O_3$-s reference and bulk MoS_2, which agrees with the prevalence of few-atom clusters. Remarkably, the Mo-Mo and Mo-S bonds shortening is the strongest for the TiO_2- and AC- supported catalysts, for which the dispersion is the highest (Table 2). As compared with the component 3, in the final state the Mo-S and Mo-Mo CNs are lesser, suggesting that MoS_3-like species lose sulfur, but also form smaller structures (Fig. 7, Tables 2 and S3).

Overall, the structure of two identified intermediates is in a general agreement with other experimental QXAFS results.[80,81] and DFT calculations[77] for alumina- supported catalysts. However, Mo ultradispersion and variations of the support lead to significant structural differences.

Evolution of components in function of temperature

For all samples, the component 2 ("oxysulfide") appears already at room temperature (Fig. 8). During the settling down of the gas flows and before the beginning of heating (5-10 min) it raises to 20-40 % relative intensity. For Mo/AC, Mo/graphene and Mo/TiO_2 samples, the maximum fraction of the component 2 is significantly lower than the one for the component 3, suggesting that the component 3 is formed more rapidly (directly from the initial oxide, or from component 2). On the other hand, for Mo/TiO_2 the component 2 remains present even when the component 3 is completely consumed, which means that the component 4 ("MoS_2") is formed directly from the component 2 ("oxysulfide"). With this respect, there is a striking difference between "weakly interacting" carbons and "strongly interacting" TiO_2, on which oxysulfide persists almost up to the end of the temperature ramp.

The MoS_2-like component 4 appears already above 100°-150° C for all samples, except carbons, where it appears above 200° C. In the previous work by Rochet et al,[40] sulfidation of the 5 wt% Mo/Al_2O_3 catalyst occurred as almost perfect 1 => 2 => 3 => 4 transformation, in which MoS_2 was produced from the component 3 only, above 200 °C. In our case, consecutive – parallel transformations were observed, in which the component 4 appeared when the components 1 and 2 were still important. Only for carbon supports almost pure component 3 is formed at 220 °C and then rapidly transformed into 4 above 300-320° C. It suggests that for the "weakly interacting" carbons relatively free-standing MoS_3 is more stable than similar species smeared over an oxide.

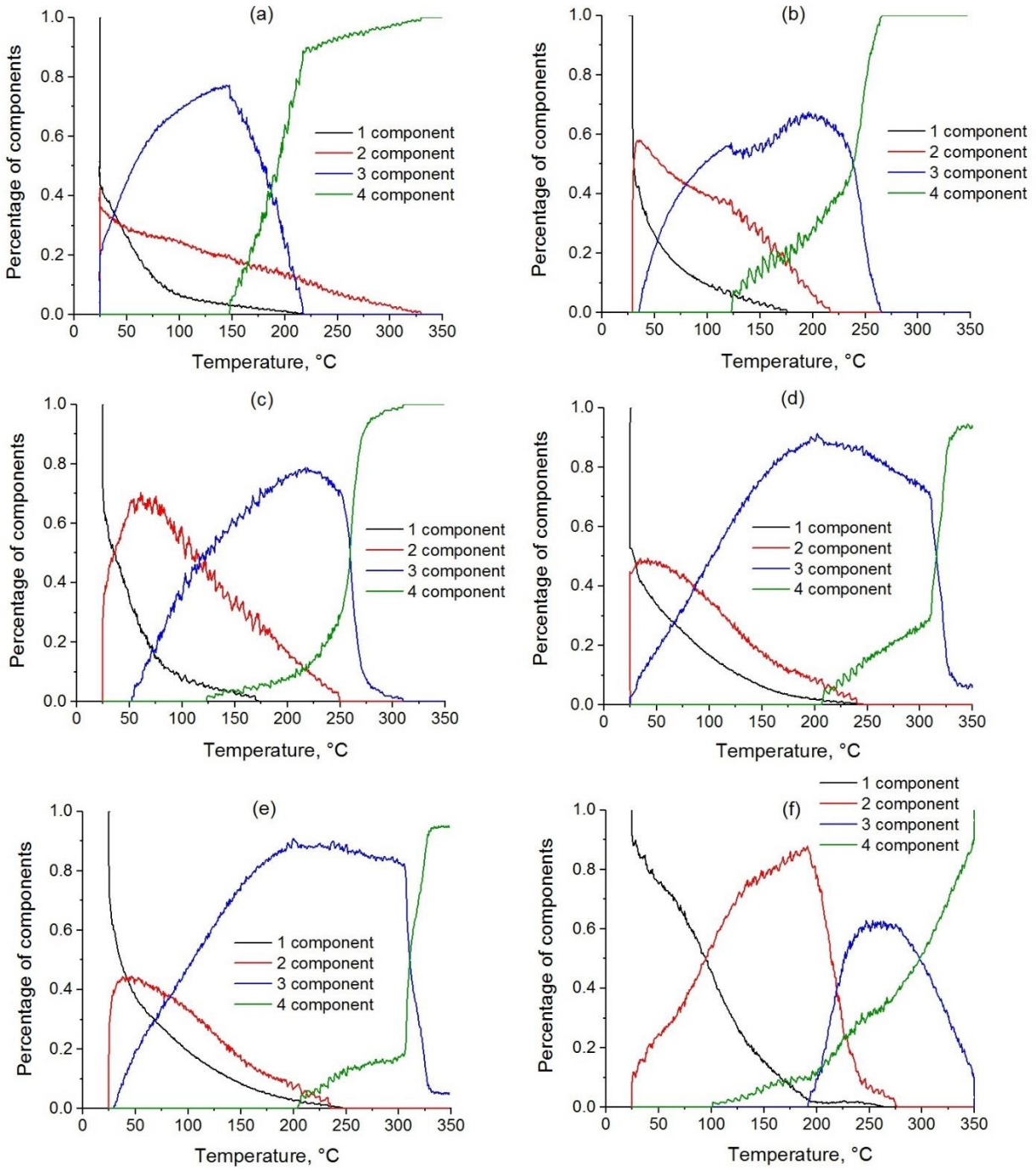

Figure 8. Evolution of molar fractions of the components vs temperature (a) Mo/TiO_2 (b) Mo/Al_2O_3 (c) Mo-KIT-6 (d) Mo/graphene (e) Mo/AC (f) ref 10Mo/Al_2O_3.

In conclusion, the nature of the support has a strong influence on the relative kinetics of the sulfidation steps. Oxysulfide intermediate tends to have higher concentrations and/or to survive longer on the oxide supports. On the contrary, the sulfur-rich component 3 is more stable on the weakly interacting carbon supports. A consecutive-parallel transformation occurs for our samples potentially involving all transitions depicted in Fig. 5.

3.2.3. XAS spectra recorded during the HDS reaction

Operando QXAS of atomically dispersed catalysts gives a unique opportunity to probe on-stream evolution of the catalytic sites. Indeed, in the nanoparticulate catalysts only a minor part of Mo atoms belongs to the catalytically active edges, so the evolution of their coordination as probed by XAS could be screened by the majority of in-slab Mo atoms. On the contrary, in the atomically dispersed clusters all Mo atoms are exposed to the gaseous reactants and the variations of their coordination are expected to be much higher. Surprisingly, no significant changes of XAS spectra occurred during the HDS reaction and subsequent exposure to pure H_2 at 350 °C. The mass-spectra attested high thiophene conversions that rapidly decay during the first several hours of *operando* HDS tests (Fig. S18,19). Also, a significant decrease of HDS activity occurred during the first hours on-stream in the laboratory HDS tests (Fig. S20), which is a usual settling-down phenomenon. However, our results suggest that this process does not involve any significant reorganization of the Mo coordination. This finding might seem counterintuitive, but could be easily explained on the basis of our previous works. For a qualitative example, in both MoS_2 and MoS_3 molybdenum has the same Mo-S CN of 6, i.e. MoS_x can lose sulfur without a decrease of the coordination number. As shown earlier, during the initial period of HDS reaction MoS_2 phase loses considerable amount of hydrogenating SH groups, before reaching a steady state.[7] These SH groups are the only form of adsorbed hydrogen.[82] When two adjacent Mo-SH groups are condensed (or a Mo-$(S)_2$-Mo moiety is reduced) toward a Mo-S-Mo one, the HDS activity decreases, but the Mo-S and Mo-Mo coordination numbers remain the same. As a result, the loss of extra sulfur, while important for catalysis, is not detected by *operando* XAS.

3.3. Catalytic activity in thiophene HDS.

The HDS activity per Mo atom changes in the sequence: Mo/graphene-s ≈ Mo/AC-s > Mo/TiO_2-s > Mo-KIT-6-s > Mo/Al_2O_3-s (Fig. 9). The Mo/graphene-s and Mo/AC-s samples demonstrated the highest specific activity around 5.5 h^{-1} (thiophene molecules per Mo atom), while Mo/Al_2O_3-s was the least active, with the value of 0.94 h^{-1}. Interestingly, a decrease of catalytic activity from the beginning of the reaction (0.5 – 1 h) to the steady state (16 h) was observed: activity was divided by 2.3 and 2.8 for Mo/graphene-s and Mo/AC-s, by 4.7 for Mo-KIT-6-s and by 2.2 for Mo/Al_2O_3-s, respectively, but only by 1.3 for Mo/TiO_2-s. The HDS rates measured during the first two hours of the reaction are shown in Fig. S20. In general, the stronger is the support - active phase interaction, the lesser is the activity evolution. Indeed, the stronger is the interaction with support, the lesser is the amount of (dangling, free form interaction with the support) extra sulfur species. As explained above, the loss of extra sulfur occurs without decrease of Mo-S coordination number and escapes from the observation by *operando* XAS.

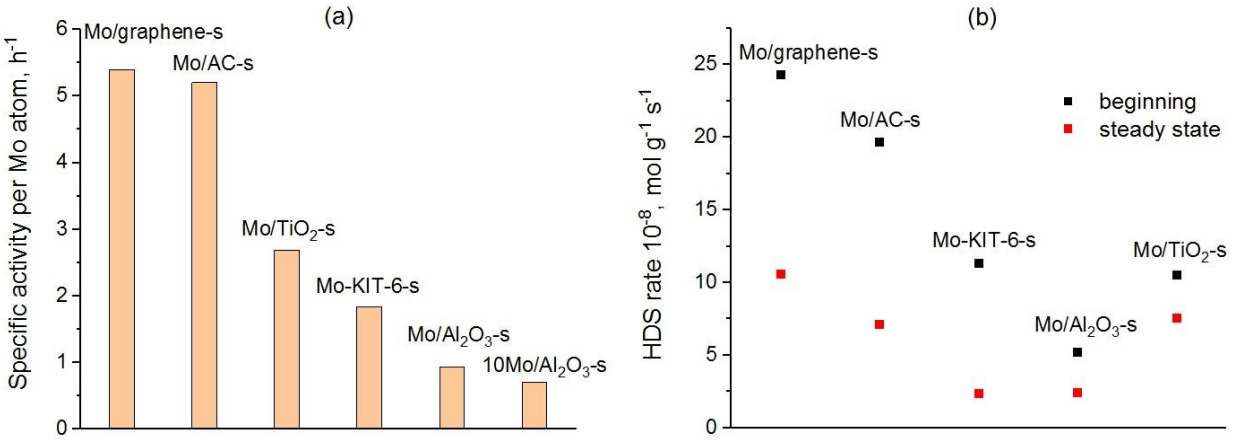

Figure 9 (a) Specific activity (per Mo atom) in HDS of thiophene at 320 °C; (b) Thiophene HDS rates (per g of catalyst) at the beginning of the reaction and in the steady state.

The main products for the oxide-supported catalysts are butenes and butane; low amounts of light hydrocarbons (mainly CH_4 and C_2H_6) were also detected (Fig. S21). Mo/TiO_2-s possesses high overall activity and the highest hydrogenating ability in agreement with the previous results.[83,84] The products distribution for Mo-KIT-6-s and Mo/Al_2O_3-s is similar, only the amount of light products (mostly, C1-C2) is higher for KIT-6. The product distribution is different for carbonaceous supports: significant amounts of propane being formed instead of the C1-C2 products. Isobutane was also spotted, nevertheless butenes remain the main products. The amount of light products in all cases diminishes with time. Such variations might be related to secondary processes that occur on the acid sites of supports and are beyond the scope of our study.

3.4. Discussion

The relationship between the properties of the support, the Mo dispersion and the HDS catalytic activity appears to be not straightforward. There is no single descriptor property (surface area, acidity, number of OH groups...) that would allow predicting better supports. No correlation between the intrinsic activity and the loading per square nm of support (Table S4) could be inferred. The two carbon-supported samples are the most active and show the highest dispersion of active species. In general, carbon is considered as a "weakly interacting" support which favors mobility and aggregation of Mo species leading to high sulfidation degree and formation large slabs of equilibrium triangular and hexagonal shape.[85,86] However, high specific surface area is favorable for high dispersion of Mo species, whereas weak sulfide-support interaction leads to a greater number of active sites than on alumina.[87] As with the difference between two carbon supports, activated carbon possesses functional groups[88] that probably decrease the Mo mobility and favor dispersion on Mo/AC-s even more than in case of Mo/graphene-s. Notably, despite the highest dispersion, the HDS activity of Mo/AC-s is not the highest but is slightly lower than for

Mo/graphene-s (Fig. 10). It seems possible that single atomic sulfide species present in the Mo/AC-s sample are not active in HDS, but a minimal oligomeric structure (at least a dimer or a trimer) is necessary for the dissociative adsorption of hydrogen and for the thiophene HDS.

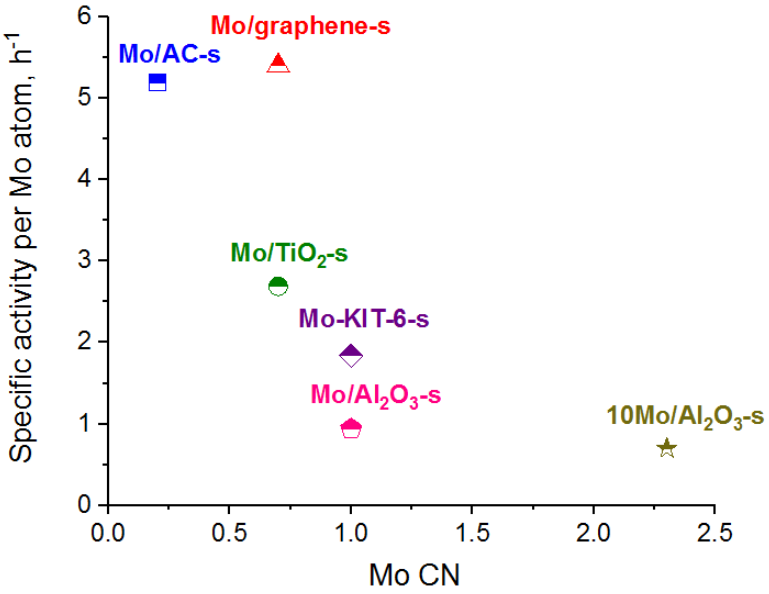

Figure 10 Dependence between the catalytic activity and Mo-Mo coordination number, determined from EXAFS of sulfided samples.

Unlikely to carbons, ultradispersed Mo species on TiO_2 are stabilized by interaction with the oxide surface. Having similar Mo-Mo CN, the Mo species on the strongly interacting TiO_2 are intrinsically less active than on carbons, but more still active than on silica and alumina, in agreement with the previous studies.[89] Beside increased dispersion, the electronic interactions seem to play an important role: theoretical calculations suggest that under HDS conditions, TiO_2 surfaces stabilize more sulfur-deficient MoS_x clusters than alumina surfaces.[90] According to the EXAFS results, MoS_x clusters possess similar structure on silica and on alumina, with a dispersion lower than on carbons and titania. Overall, the HDS activity follows a general correlation with dispersion (Fig. 10), but specific chemical interactions seem also to play an important role.

The advantage of ultradispersed catalysts over the corresponding 10%wt Mo references in terms of per Mo atom HDS activity appears to depend on the nature of the support. For carbon supports, the ultradispersed catalysts have more than twice higher intrinsic activity than the conventional 10 % wt. Mo systems (Fig. S22). For the oxide-supported systems this ratio is lower, being 1.7 for TiO_2 and 1.4 for Al_2O_3. If we suppose that all Mo atoms in the highly-loaded catalysts are present only in the form of slabs, whereas the TOF of exposed Mo atoms at the edges and in the small clusters is the same, then the expected activity ratio between them should be around 3 (because in the highly dispersed supported MoS2 slabs about 1/3 of Mo atoms are exposed at the edges,[8] whereas we suppose that all Mo atoms are exposed in the small clusters). The observed

activity ratios in Fig S22 are lower than 3, which is naturally explained by the presence of significant amounts of few-atom clusters even in the high-loaded catalysts. The difference of the intrinsic activity between the high-loaded and low-loaded samples in function of the support probably depends on the distribution of Mo species between the few-atom clusters and the slabs. It would be highly instructive to follow such distribution as a function of the support and of the loading, but that remains beyond the frames of the present study.

4. Conclusions

We prepared ultradispersed MoS_x species on different supports, including carbons, silica, titania and alumina and confirmed atomic dispersion by characterizations (TEM, STEM, Raman, UV-vis DRS). Such catalysts show high intrinsic (per Mo atom) HDS activity in the absence of significant amounts of MoS_2 slabs. The intrinsic HDS activity of ultradispersed catalysts is always superior to the conventional 10 wt% Mo references. This gain of activity is the highest for the carbon supports and the lowest for alumina. The ratio of intrinsic activity between low-loaded and 10 %wt Mo is probably dependent on the distribution of molybdenum between the small clusters and the slabs, which is in turn determined by the nature of support, namely by the strength of interaction with Mo species. If follows from our results that for any sulfide catalyst, independently on the support and the loading, TEM-invisible subnanomertic clusters potentially provide a significant contribution to the observed HDS activity. The amount and the stability of ultradispersed species would obviously vary in function of the support nature, the Mo loading and the conditions. Previously overlooked, the contribution of ultradispersed species is therefore accountable for a considerable part of the phenomena known as “support effect”. Though specific chemical support effects seem to be significant, a general correlation exists between the dispersion of MoS_x species and their intrinsic HDS activity.

By means of *operando* QXAS study we demonstrated that evolution of ultradispersed MoS_x species during the sulfidation process occurs via a subsequent – parallel pathway including oxysulfide and MoS_3-like intermediates. However, the structure of these intermediates and their relative stability is affected by the nature of support. The structure of fully sulfided MoS_x species depends on the support. While MoS_2 –like clusters are formed on silica and alumina, the MoS_x species are significantly different on carbons and titania. As the kinetics of the components transformation is substantially different for different supports, in the further work it seems possible to build reaction kinetic models for these components and to extract energies of transformations, in order to compare them with the ab initio calculations.

Acknowledgements

This work was supported by a public grant overseen by the French National Research Agency (ANR) as a part of the "Investissements d'Avenir" (ref: ANR-10-EQPX-45) provided for the building of the ROCK beamline.

References

[1] Topsøe, H.; Clausen, B.S.; Massoth, F.E. "Hydrotreating Catalysis Science and Technology", Springer-Verlag New York, 1996. ISBN No. 3-540-60380-8 pp 1–269.
[2] Šarić, M.; Rossmeisl, J.; Moses, P. G. Modeling the Adsorption of Sulfur Containing Molecules and Their Hydrodesulfurization Intermediates on the Co-Promoted MoS_2 Catalyst by DFT. J. Catal. 2018, 358, 131–140.
[3] Lauritsen, J. V.; Helveg, S.; Lægsgaard, E.; Stensgaard, I.; Clausen, B. S.; Topsøe, H.; Besenbacher, F. Atomic-Scale Structure of Co–Mo–S Nanoclusters in Hydrotreating Catalysts. J. Catal. 2001, 197 (1), 1–5.
[4] Krebs, E.; Silvi, B.; Daudin, A.; Raybaud, P. A DFT Study of the Origin of the HDS/HydO Selectivity on Co(Ni)MoS Active Phases. J.Catal. 2008, 260 (2), 276–287.
[5] Raybaud, P.; Hafner, J.; Kresse, G.; Toulhoat, H. Structural and Electronic Properties of the $MoS_2(10\bar{1}0)$ Edge-Surface. Surf. Sci. 1998, 407 (1), 237–250.
[6] Chen, J.; Dominguez Garcia, E.; Oliviero, E.; Oliviero, L.; Maugé, F. Effect of high pressure sulfidation on the morphology and reactivity of MoS_2 slabs on MoS_2/Al_2O_3 catalyst prepared with citric acid, J. Catal. 2016, 339, 153–162.
[7] Afanasiev, P. The influence of reducing and sulfiding conditions on the properties of unsupported MoS_2-based catalysts, J. Catal. 2010, 269, 269–280.
[8] Baubet, B.; Devers, E.; Hugon, A.; Leclerc, E.; Afanasiev, P. The Influence of MoS_2 Slab 2D Morphology and Edge State on the Properties of Alumina-Supported Molybdenum Sulfide Catalysts. Appl. Catal. A: Gen. 2014, 487, 72–81.
[9] Baubet, B.; Girleanu, M.; Gay, A.-S.; Taleb, A.-L.; Moreaud, M.; Wahl, F.; Delattre, V.; Devers, E.; Hugon, A.; Ersen, O.; Afanasiev, P.; Raybaud, P. Quantitative Two-Dimensional (2D) Morphology–Selectivity Relationship of CoMoS Nanolayers: A Combined High-Resolution High-Angle Annular Dark Field Scanning Transmission Electron Microscopy (HR HAADF-STEM) and Density Functional Theory (DFT) Study. ACS Catal. 2016, 6 (2), 1081–1092.
[10] Zavala-Sanchez, L.; Portier, X.; Maugé, F.; Oliviero, L. Formation and Stability of CoMoS Nanoclusters by the Addition of Citric Acid: A Study by High Resolution STEM-HAADF Microscopy. Catal. Today 2021, 377, 127–134.
[11] Girleanu, M.; Lopes Silva, S.; Ihiawakrim, D.; Chaumonnot, A.; Bonduelle-Skrzypczak, A.; Lefebvre, F.; Dufaud, V.; Gay, A.-S.; Ersen, O. HAADF-STEM High-Resolution Study of Nanometric MoS_2 inside Mesoporous SBA-15. Micropor. Mesopor. Mat. 2015, 217, 190–195.
[12] Ryaboshapka, D.; Piccolo, L.; Aouine, M.; Bargiela, P.; Briois, V.; Afanasiev, P. Ultradispersed (Co)Mo Catalysts with High Hydrodesulfurization Activity. Appl. Catal. B: Environ. 2022, 302, 120831.
[13] Breysse, M.; Afanasiev, P.; Geantet, C.; Vrinat, M. Overview of Support Effects in Hydrotreating Catalysts. Catal. Today 2003, 86 (1), 5–16.
[14] Hensen, E. J. M.; Kooyman, P. J.; van der Meer, Y.; van der Kraan, A. M.; de Beer, V. H. J.; van Veen, J. A. R.; van Santen, R. A. The Relation between Morphology and Hydrotreating Activity for Supported MoS_2 Particles. J. Catal. 2001, 199 (2), 224–235.
[15] Pratt, K. Morphology and activity of MoS_2 on various supports: Genesis of the active phase, J. Catal. 1990, 124(2) 416–432.
[16] Gutiérrez, O. Y.; Singh, S.; Schachtl, E.; Kim, J.; Kondratieva, E.; Hein, J.; Lercher, J. A. Effects of the Support on the Performance and Promotion of (Ni)MoS_2 Catalysts for Simultaneous Hydrodenitrogenation and Hydrodesulfurization. ACS Catal. 2014, 4 (5), 1487–1499.
[17] Breysse, M.; Portefaix, J. L.; Vrinat, M. Support Effects on Hydrotreating Catalysts. Catal. Today 1991, 10(4), 489–505.
[18] Payen, E.; Hubaut, R.; Kasztelan, S.; Poulet, O.; Grimblot, J. Morphology Study of MoS_2- and WS_2-Based Hydrotreating Catalysts by High-Resolution Electron Microscopy. J. Catal.1994, 147 (1), 123–132.
[19] Kibsgaard, J.; Clausen, B. S.; Topsøe, H.; Lægsgaard, E.; Lauritsen, J. V.; Besenbacher, F. Scanning Tunneling Microscopy Studies of TiO_2-Supported Hydrotreating Catalysts: Anisotropic Particle Shapes by Edge-Specific MoS_2–Support Bonding. J. Catal. 2009, 263 (1), 98–103.
[20] Ninh, T. K. T.; Laurenti, D.; Leclerc, E.; Vrinat, M. Support Effect for CoMoS and CoNiMoS Hydrodesulfurization Catalysts Prepared by Controlled Method. Appl. Catal. A: Gen. 2014, 487, 210–218.

[21] Nguyen, M.-T.; Tayakout-Fayolle, M.; Chainet, F.; Pirngruber, G. D.; Geantet, C. Use of Kinetic Modeling for Investigating Support Acidity Effects of NiMo Sulfide Catalysts on Quinoline Hydrodenitrogenation. Appl. Catal. A: Gen. 2017, 530, 132–144.
[22] Blanchard, J.; Breysse, M.; Fajerwerg, K.; Louis, C.; Hédoire, C.-E.; Sampieri, A.; Zeng, S.; Pérot, G.; Nie, H.; Li, D. Acidic Zeolites and Al-SBA-15 as Supports for Sulfide Phases: Application to Hydrotreating Reactions. In Stud. Surf. Sci. Catal.; Čejka, J., Žilková, N., Nachtigall, P., Eds.; Molecular Sieves: From Basic Research to Industrial Applications; Elsevier, 2005; Vol. 158, pp 1517–1524.
[23] Dominguez Garcia, E.; Chen, J.; Oliviero, E.; Oliviero, L.; Maugé, F. New Insight into the Support Effect on HDS Catalysts: Evidence for the Role of Mo-Support Interaction on the MoS_2 Slab Morphology. Appl. Catal. B: Env. 2020, 260, 117975.
[24] Kaluža, L.; Gulková, D.; Vít, Z.; Zdražil, M. Effect of Support Type on the Magnitude of Synergism and Promotion in CoMo Sulphide Hydrodesulphurisation Catalyst. Appl. Catal. A: Gen. 2007, 324, 30–35.
[25] Garcia de Castro, R.; Devers, E.; Digne, M.; Lamic-Humblot, A.-F.; Pirngruber, G. D.; Carrier, X. Surface-Dependent Activity of Model CoMoS Hydrotreating Catalysts. J. Catal. 2021, 403, 16–31.
[26] Galhenage, R. P.; Yan, H.; Rawal, T. B.; Le, D.; Brandt, A. J.; Maddumapatabandi, T. D.; Nguyen, N.; Rahman, T. S.; Chen, D. A. MoS_2 Nanoclusters Grown on TiO_2: Evidence for New Adsorption Sites at Edges and Sulfur Vacancies. J. Phys. Chem. C 2019, 123 (12), 7185–7201.
[27] Lee, M.; Kim, Y.; Mohamed, A. Y.; Lee, H.-K.; Ihm, K.; Kim, D. H.; Park, T. J.; Cho, D.-Y. Direct Evidence of Electronic Interaction at the Atomic-Layer-Deposited MoS_2 Monolayer/SiO_2 Interface. ACS Appl. Mater. Interf. 2020, 12 (48), 53852–53859.
[28] Grunwaldt, J.-D.; Caravati, M.; Hannemann, S.; Baiker, A. X-ray absorption spectroscopy under reaction conditions: suitability of different reaction cells for combined catalyst characterization and time-resolved studies. Phys. Chem. Chem. Phys. 2004, 6, 3037−3047.
[29] Browne, V. M.; Louwers, S. P. A.; Prins, R. The Effect of Passivation on the Activity of Sulfided Mo and Co-Mo Hydrodesulphurization Catalysts. Catal. Today 1991, 10 (3), 345–352.
[30] Geantet, C.; Soldo, Y.; Glasson, C.; Matsubayashi, N.; Lacroix, M.; Proux, O.; Ulrich, O.; Hazemann, J.-L. In Situ QEXAFS Investigation at Co K-Edge of the Sulfidation of a CoMo/Al_2O_3 Hydrotreating Catalyst. Catal. Lett. 2001, 73 (2), 95–98.
[31] Plais, L.; Lancelot, C.; Lamonier, C.; Payen, E.; Briois, V. First in situ temperature quantification of CoMoS species upon gas sulfidation enabled by new insight on cobalt sulfide formation. Catal. Today 2021, 377, 114−126
[32] Gajdek, D.; Jensen, L. I. A.; Briois, V.; Hulteberg, C.; Merte, L. R.; Blomberg, S. Sulfidation of Supported Ni, Mo and NiMo Catalysts Studied by In Situ XAFS. Top Catal 2023. https://doi.org/10.1007/s11244-023-01781-z.
[33] Len, T.; Bahri, M.; Ersen, O.; Lefkir, Y.; Cardenas, L.; Villar-Garcia, I. J.; Pérez Dieste, V.; Llorca, J.; Perret, N.; Checa, R.; Puzenat, E.; Afanasiev, P.; Morfin, F.; Piccolo, L. Ultradispersed Mo/TiO_2 Catalysts for CO_2 Hydrogenation to Methanol. Green Chem. 2021, 23 (18), 7259–7268.
[34] Afanasiev, P. Calculation of MoS_2 Slabs Morphology Descriptors from Transmission Electron Microscopy Data Revisited. Case Study of the Influence of Citric Acid and Treatment Conditions on the Properties of MoS_2/Al_2O_3. Appl. Catal. A: Gen. 2017, 529, 10–19.
[35] Chen, P.; Xie, Z.; Zhao, Z.; Li, J.; Liu, B.; Liu, B.; Fan, X.; Kong, L.; Xiao, X. Study on the Selective Oxidation of Methane over Highly Dispersed Molybdenum-Incorporated KIT-6 Catalysts. Catal. Sci. Technol. 2021, 11(12), 4083–4097.
[36] Briois, V.; La Fontaine, C.; Belin, S.; Barthe, L.; Moreno, T.; Pinty, V.; Carcy, A.; Girardot, R.; Fonda, E. ROCK: The New Quick-EXAFS Beamline at SOLEIL. J. Phys.: Conf. Ser. 2016, 712, 012149.
[37] La Fontaine, C.; Barthe, L.; Rochet, A.; Briois, V. X-Ray Absorption Spectroscopy and Heterogeneous Catalysis: Performances at the SOLEIL's SAMBA Beamline. Catal. Today 2013, 205, 148–158.
[38] Ankudinov, A. L.; Ravel, B.; Rehr, J. J.; Conradson, S. D. Real-Space Multiple-Scattering Calculation and Interpretation of x-Ray-Absorption near-Edge Structure. Phys. Rev. B 1998, 58(12), 7565–7576.
[39] Klementev, K. V. Extraction of the Fine Structure from X-Ray Absorption Spectra. J. Phys. D: Appl. Phys. 2001, 34 (2), 209.
[40] Rochet, A.; Baubet, B.; Moizan, V.; Pichon, C.; Briois, V. Co-K and Mo-K Edges Quick-XAS Study of the Sulphidation Properties of Mo/Al_2O_3 and CoMo/Al_2O_3 Catalysts. C. R. Chim. 2016, 19(10), 1337–1351.
[41] Lesage, C.; Devers, E.; Legens, C.; Fernandes, G.; Roudenko, O.; Briois, V. High Pressure Cell for Edge Jumping X-Ray Absorption Spectroscopy: Applications to Industrial Liquid Sulfidation of Hydrotreatment Catalysts. Catal. Today 2019, 336, 63–73.
[42] Jaumot, J.; de Juan, A.; Tauler, R. MCR-ALS GUI 2.0: New Features and Applications. Chemometr. Intell. Lab. Syst. 2015, 140, 1–12.
[43] Blanchet, L. Méthodes de résolution dédiées à l'étude spectroscopique de processus photoinduits. Adaptation aux spécificités des spectres résolus en temps, PhD thesis, Université des Sciences et Technologie de Lille - Lille I, 2008.
[44] Wieting, T. J.; Verble, J. L. Infrared and Raman Studies of Long-Wavelength Optical Phonons in Hexagonal MoS_2. Phys. Rev. B 1971, 3 (12), 4286–4292.
[45] Yaremko, A. M.; Yukhymchuk, V. O.; Romanyuk, Y. A.; Baran, J.; Placidi, M. Theoretical and Experimental Study of Phonon Spectra of Bulk and Nano-Sized MoS_2 Layer Crystals. Nanoscale Res. Lett. 2017, 12 (1), 82.

[46] Blanco, É.; Afanasiev, P.; Berhault, G.; Uzio, D.; Loridant, S. Resonance Raman Spectroscopy as a Probe of the Crystallite Size of MoS_2 Nanoparticles. C. R. Chimie 2016, 19 (10), 1310–1314.
[47] Schrader, G. L.; Cheng, C. P. In Situ Laser Raman Spectroscopy of the Sulfiding of Moγ-Al_2O_3 Catalysts. J. Catal. 1983, 80 (2), 369–385.
[48] Jeziorowski, H.; Knoezinger, H. Raman and Ultraviolet Spectroscopic Characterization of Molybdena on Alumina Catalysts. J. Phys. Chem. 1979, 83 (9), 1166–1173.
[49] Catita, L.; Quoineaud, A.-A.; Espinat, D.; Pichon, C.; Delpoux, O. Application of Magnetic Resonance Imaging and Raman Imaging to Study the Impact of Phosphorus in Impregnation of Hydrotreatment Catalysts. Appl. Catal. A: Gen. 2017, 547, 164–175.
[50] Rusciano, G.; Capaccio, A.; Sasso, A.; Singh, M.; Valadan, M.; Dell'Aversana, C.; Altucci, L.; Altucci, C. Single-Cell Photothermal Analysis Induced by MoS_2 Nanoparticles by Raman Spectroscopy. Front. Bioeng. Biotech. 2022, 10, 1-10.
[51] Forsberg, V.; Zhang, R.; Bäckström, J.; Dahlström, C.; Andres, B.; Norgren, M.; Andersson, M.; Hummelgård, M.; Olin, H. Exfoliated MoS_2 in Water without Additives. PLoS ONE 2016, 11, e0154522.
[52] J. Wang, L. Chen, W. Lu, M. Zeng, L. Tan, F. Ren, C. Jiang, L. Fu, Direct growth of molybdenum disulfide on arbitrary insulating surfaces by chemical vapor deposition, RSC Adv. 5 (2015) 4364–4367.
[53] Cesano, F.; Bertarione, S.; Piovano, A.; Agostini, G.; Mastabur Rahman, M.; Groppo, E.; Bonino, F.; Scarano, D.; Lamberti, C.; Bordiga, S.; Montanari, L.; Bonoldi, L.; Millini, R.; Zecchina, A. Model Oxide Supported MoS_2 HDS Catalysts: Structure and Surface Properties. Catal. Sci. Technol. 2011, 1 (1), 123–136.
[54] Afanasiev, P. MoS_2 "Inorganic Fullerenes" Combined with TiO_2 in Water-Methanol Suspensions: Highly Active Hydrogen Production Photo Catalysts Operating via Transfer of Accumulated Electrons. Int. J. Hydr. Energy 2020, 45 (29), 14696–14712.
[55] Ghayeb Zamharir, S.; Karimzadeh, R.; Aboutalebi, S. H. Laser-Assisted Tunable Optical Nonlinearity in Liquid-Phase Exfoliated MoS_2 Dispersion. Appl. Phys. A 2018, 124 (10), 692.
[56] Ko, T. Y.; Jeong, A.; Kim, W.; Lee, J.; Kim, Y.; Lee, J. E.; Ryu, G. H.; Park, K.; Kim, D.; Lee, Z.; Lee, M. H.; Lee, C.; Ryu, S. On-Stack Two-Dimensional Conversion of MoS_2 into MoO_3. 2D Mater. 2016, 4 (1), 014003.
[57] Plais, L. Catalyseurs d'hydrotraitement Mo/Al_2O_3 doublement promus preparés à partir d'hétéropolyanions d'Anderson: Suivi de la sulfuration par Quick-EXAFS, PhD thesis, University of Lille, 2017
[58] Wang, H. W.; Skeldon, P.; Thompson, G. E. XPS Studies of MoS_2 Formation from Ammonium Tetrathiomolybdate Solutions. Surf. Coat. Technol. 1997, 91 (3), 200–207.
[59] Schauble, K.; Zakhidov, D.; Yalon, E.; Deshmukh, S.; Grady, R. W.; Cooley, K. A.; McClellan, C. J.; Vaziri, S.; Passarello, D.; Mohney, S. E.; Toney, M. F.; Sood, A. K.; Salleo, A.; Pop, E. Uncovering the Effects of Metal Contacts on Monolayer MoS_2. ACS Nano 2020, 14 (11), 14798–14808.
[60] Qie, L.; Chen, W.; Xiong, X.; Hu, C.; Zou, F.; Hu, P.; Huang, Y. Sulfur-Doped Carbon with Enlarged Interlayer Distance as a High-Performance Anode Material for Sodium-Ion Batteries. Adv. Sci. 2015, 2(12) 1500195
[61] Carrier, X.; Lambert, J. F.; Che, M. Ligand-Promoted Alumina Dissolution in the Preparation of MoO_x /γ-Al_2O_3 Catalysts: Evidence for the Formation and Deposition of an Anderson-Type Alumino Heteropolymolybdate. J. Am. Chem. Soc. 1997, 119 (42), 10137–10146.
[62] Dou, J.; Zeng, H. C. Targeted Synthesis of Silicomolybdic Acid (Keggin Acid) inside Mesoporous Silica Hollow Spheres for Friedel–Crafts Alkylation. J. Am. Chem. Soc. 2012, 134 (39), 16235–16246.
[63] Nikulshina, M.; Mozhaev, A.; Lancelot, C.; Marinova, M.; Blanchard, P.; Payen, E.; Lamonier, C.; Nikulshin, P. MoW Synergetic Effect Supported by HAADF for Alumina Based Catalysts Prepared from Mixed $SiMo_nW_{12-n}$ Heteropolyacids. Appl. Catal. B: Env. 2018, 224, 951–959.
[64] Kim, D. S.; Wachs, I. E.; Segawa, K. Molecular Structures and Reactivity of Supported Molybdenum Oxide Catalysts. J. Catal. 1994, 149 (2), 268–277.
[65] Hu, H.; Wachs, I. E.; Bare, S. R. Surface Structures of Supported Molybdenum Oxide Catalysts: Characterization by Raman and Mo L3-Edge XANES. J. Phys. Chem. 1995, 99 (27), 10897–10910.
[66] Tougerti, A.; Berrier, E.; Mamede, A.-S.; La Fontaine, C.; Briois, V.; Joly, Y.; Payen, E.; Paul, J.-F.; Cristol, S. Synergy between XANES Spectroscopy and DFT to Elucidate the Amorphous Structure of Heterogeneous Catalysts: TiO_2-Supported Molybdenum Oxide Catalysts. Angew. Chem., Int. Ed. 2013, 52 (25), 6440–6444.
[67] Hu, H.; Oliveira de Souza, D.; Berrier, E.; Paul, J.-F.; La Fontaine, C.; Briois, V.; Cristol, S.; Tougerti, A. Investigation of the Reducibility of Supported Oxomolybdate Species for Mapping of Active Centers of Partial Oxidation Reaction: In Situ Mo K-Edge XAS and DFT Study. J. Phys. Chem. C 2019, 123 (30), 18325–18335.
[68] Kang, J. H.; Menard, L. D.; Nuzzo, R. G.; Frenkel, A. I. Unusual Non-Bulk Properties in Nanoscale Materials: Thermal Metal−Metal Bond Contraction of γ-Alumina-Supported Pt Catalysts. J. Am. Chem. Soc. 2006, 128 (37), 12068–12069.
[69] Wu, L.; Longo, A.; Dzade, N. Y.; Sharma, A.; Hendrix, M. M. R. M.; Bol, A. A.; de Leeuw, N. H.; Hensen, E. J. M.; Hofmann, J. P. The Origin of High Activity of Amorphous MoS_2 in the Hydrogen Evolution Reaction. ChemSusChem 2019, 12 (19), 4383–4389.
[70] Afanasiev, P.; Jobic, H.; Lorentz, C.; Leverd, P.; Mastubayashi, N.; Piccolo, L.; Vrinat, M. Low-Temperature Hydrogen Interaction with Amorphous Molybdenum Sulfides MoS_x. J. Phys. Chem. C 2009, 113 (10), 4139–4146.
[71] Kouzu, M.; Kuriki, Y.; Hamdy, F.; Sakanishi, K.; Sugimoto, Y.; Saito, I. Catalytic Potential of Carbon-Supported NiMo-Sulfide for Ultra-Deep Hydrodesulfurization of Diesel Fuel. Appl. Catal. A: Gen. 2004, 265 (1), 61–67.

[72] Ramirez, J.; Fuentes, S.; Díaz, G.; Vrinat, M.; Breysse, M.; Lacroix, M. Hydrodesulphurization Activity and Characterization of Sulphided Molybdenum and Cobalt—Molybdenum Catalysts: Comparison of Alumina-, Silica-Alumina- and Titania-Supported Catalysts. Appl. Catal. 1989, 52 (1), 211–224.
[73] Abotsi, G. M. K.; Scaroni, A. W. A Review of Carbon-Supported Hydrodesulfurization Catalysts. Fuel Processing Technol. 1989, 22 (2), 107–133.
[74] Weber, Th.; Muijsers, J. C.; van Wolput, J. H. M. C.; Verhagen, C. P. J.; Niemantsverdriet, J. W. Basic Reaction Steps in the Sulfidation of Crystalline MoO_3 to MoS_2, As Studied by X-Ray Photoelectron and Infrared Emission Spectroscopy. J. Phys. Chem. 1996, 100 (33), 14144–14150.
[75] Texier, S.; Berhault, G.; Pérot, G.; Diehl, F. Activation of Alumina-Supported Hydrotreating Catalysts by Organosulfides or H_2S: Effect of the H_2S Partial Pressure Used during the Activation Process. Applied Catalysis A: General 2005, 293, 105–119.
[76] de Jong, A. M.; Borg, H. J.; van IJzendoorn, L. J.; Soudant, V. G. F. M.; de Beer, V. H. J.; van Veen, J. A. R.; Niemantsverdriet, J. W. Sulfidation Mechanism by Molybdenum Catalysts Supported on Silica/Silicon(100) Model Support Studied by Surface Spectroscopy. J. Phys. Chem. 1993, 97 (24), 6477–6483.
[77] Sahu, A.; Steinmann, S. N.; Raybaud, P. Genesis of MoS_2 from model-Mo-oxide precursors supported on γ-alumina, J. Catal. 2022, 408, 303–315.
[78] Leliveld, R. G.; van Dillen, A. J.; Geus, J. W.; Koningsberger, D. C. A Mo–K Edge XAFS Study of the Metal Sulfide-Support Interaction in (Co)Mo Supported Alumina and Titania Catalysts. J. Catal. 1997, 165 (2), 184–196.
[79] McDonald, J. W.; Friesen, G. D.; Rosenhein, L. D.; Newton, W. E. Syntheses and Characterization of Ammonium and Tetraalkylammonium Thiomolybdates and Thiotungstates. Inorg. Chim. Acta 1983, 72, 205–210.
[80] Rochet, A.; Baubet, B.; Moizan, V.; Devers, E.; Hugon, A.; Pichon, C.; Payen, E.; Briois, V. Intermediate Species Revealed during Sulfidation of Bimetallic Hydrotreating Catalyst: A Multivariate Analysis of Combined Time-Resolved Spectroscopies. J. Phys. Chem. C 2017, 121 (34), 18544–18556.
[81] Nikulshina, M.; Blanchard, P.; Lancelot, C.; Griboval-Constant, A.; Marinova, M.; Briois, V.; Nikulshin, P.; Lamonier, C. Genesis of Active Phase in MoW/Al_2O_3 Hydrotreating Catalysts Monitored by HAADF and in Situ QEXAFS Combined to MCR-ALS Analysis. Appl. Catal. B: Env. 2020, 269, 118766.
[82] Afanasiev, P. Jobic, H. On hydrogen adsorption by nanodispersed MoS_2-based catalysts, J. Catal. 2021, 403, 111–120.
[83] Escobar, J.; Toledo, J. A.; Cortés, M. A.; Mosqueira, M. L.; Pérez, V.; Ferrat, G.; López-Salinas, E.; Torres-García, E. Highly Active Sulfided CoMo Catalyst on Nano-Structured TiO_2. Catal. Today 2005, 106 (1–4), 222–226.
[84] Signorile, M.; Damin, A.; Budnyk, A.; Lamberti, C.; Puig-Molina, A.; Beato, P.; Bordiga, S. MoS_2 supported on P25 titania: A model system for the activation of a HDS catalyst, J. Catal. 2015, 328, 225–235.
[85] Brorson, M.; Carlsson, A.; Topsøe, H. The Morphology of MoS2, WS2, Co–Mo–S, Ni–Mo–S and Ni–W–S Nanoclusters in Hydrodesulfurization Catalysts Revealed by HAADF-STEM. Catal. Today 2007, 123 (1), 31–36.
[86] C. Bara, A.-F. Lamic-Humblot, E. Fonda, A.-S. Gay, A.-L. Taleb, E. Devers, M. Digne, G.D. Pirngruber, X. Carrier, Surface-dependent sulfidation and orientation of MoS_2 slabs on alumina-supported model HDS catalysts, J. Catal. 344 (2016) 591-605.
[87] Kogan, V. M.; Rozhdestvenskaya, N. N. ^{35}S Tracer Study of the Effect of Support on the Nature of the Active Sites of Co(Ni)Mo Sulphide Catalysts Supported on Al_2O_3 and Activated Carbon. Oil & Gas Science and Technology - Rev. IFP 2006, 61 (4), 547–559.
[88] Abotsi, G. M. K.; Scaroni, A. W. A Review of Carbon-Supported Hydrodesulfurization Catalysts. Fuel Process. Techn. 1989, 22 (2), 107–133.
[89] Wang, D.; Li, J.; Zheng, A.; Ma, H.; Pan, Z.; Qu, W.; Wang, L.; Han, J.; Wang, C.; Tian, Z. Quasi-Single-Layer MoS_2 on MoS_2/TiO_2 Nanoparticles for Anthracene Hydrogenation, ACS Appl. Nano Mater. 2019, 2 (8), 5096–5107.
[90] Arrouvel, C.; Breysse, M.; Toulhoat, H.; Raybaud, P. A density functional theory comparison of anatase (TiO_2)- and γ-Al_2O_3-supported MoS_2 catalysts, J.Catal. 2005, 232 (1), 161–178.